THE JOURNAL OF PHYSICAL CHEMISTRY B
A JOURNAL OF THE AMERICAN CHEMICAL SOCIETY

pubs.acs.org/JPCB

Article

Comparison of the Backbone Dynamics of Dehaloperoxidase-Hemoglobin Isoenzymes

Jessica M. González-Delgado, Peter M. Thompson, Witold Andrałojć, Zofia Gdaniec, Reza A. Ghiladi, and Stefan Franzen*

Cite This: *J. Phys. Chem. B* 2024, 128, 3383−3397

Read Online

ACCESS | Metrics & More | Article Recommendations | Supporting Information

ABSTRACT: Dehaloperoxidase (DHP) is a multifunctional hemeprotein with a functional switch generally regulated by the chemical class of the substrate. Its two isoforms, DHP-A and DHP-B, differ by only five amino acids and have an almost identical protein fold. However, the catalytic efficiency of DHP-B for oxidation by a peroxidase mechanism ranges from 2- to 6-fold greater than that of DHP-A depending on the conditions. X-ray crystallography has shown that many substrates and ligands have nearly identical binding in the two isoenzymes, suggesting that the difference in catalytic efficiency could be due to differences in the conformational dynamics. We compared the backbone dynamics of the DHP isoenzymes at pH 7 through heteronuclear relaxation dynamics at 11.75, 16.45, and 19.97 T in combination with four 300 ns MD simulations. While the overall dynamics of the isoenzymes are similar, there are specific local differences in functional regions of each protein. In DHP-A, Phe35 undergoes a slow chemical exchange between two conformational states likely coupled to a swinging motion of Tyr34. Moreover, Asn37 undergoes fast chemical exchange in DHP-A. Given that Phe35 and Asn37 are adjacent to Tyr34 and Tyr38, it is possible that their dynamics modulate the formation and migration of the active tyrosyl radicals in DHP-A at pH 7. Another significant difference is that both distal and proximal histidines have a 15−18% smaller S^2 value in DHP-B, thus their greater flexibility could account for the higher catalytic activity. The distal histidine grants substrate access to the distal pocket. The greater flexibility of the proximal histidine could also accelerate H_2O_2 activation at the heme Fe by increased coupling of an amino acid charge relay to stabilize the ferryl Fe(IV) oxidation state in a Poulos-Kraut "push−pull"-type peroxidase mechanism.

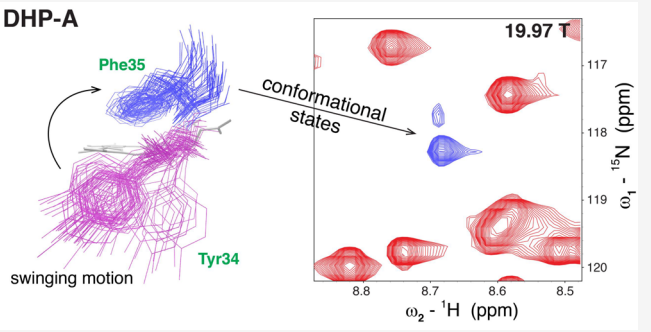

1. INTRODUCTION

The internal motions of enzymes can affect a wide range of functions such as their catalytic turnover, subunit assembly, allostery, and conformational fluctuations. For example, in hemoglobin, the binding of oxygen to one of its subunits causes a conformational change that increases its overall oxygen affinity, causing it to transition from a low-affinity *T* (tense) state to a high-affinity *R* (relaxed) state.[1,2] In the case of dehaloperoxidase-hemoglobin (DHP), its distal histidine exhibits allosteric behavior and adopts either an internal (closed) or a solvent-exposed (open) conformation upon binding of substrates or other small molecules.[3−6] This allosteric behavior allows DHP to regulate the entrance and exit of small molecules into its distal cavity. DHP is a peroxidase enzyme that contains a typical globin fold with an iron protoporphyrin IX cofactor and primarily acts as an oxygen transport enzyme in the marine polychaete worm *Amphitrite ornata*.[7,8] It is a multifunctional hemeprotein that can also carry out peroxidase, peroxygenase, oxidase, and oxygenase functions depending on the chemical class of the substrate (e.g., phenols, indoles, guaiacols, cresols, etc.).[7−11] It is hypothesized that these additional functions of DHP are adaptations by *A. ornata* to survive an environment containing toxic brominated and chlorinated phenolic compounds originating from secreted metabolites of other cohabiting organisms and byproducts of anthropogenic activities.[7,12−14] DHP can oxidize these toxic compounds and produce lower-toxicity products, acting as a detoxifying enzyme.

DHP has two isoforms, DHP-A and DHP-B (Figure 1), which have a 96.4% sequence homology and differ only by five amino acids (I9L, R32K, Y34N, N81S, and S91G).[15] Although their backbones overlay almost perfectly and possess an almost identical protein fold, DHP-B has a 2- to 6-fold greater peroxidase activity chemistry depending on substrate, buffer, and pH.[16,17] Based on kinetic assays of the peroxidase substrate

Received: October 30, 2023
Revised: January 27, 2024
Accepted: January 29, 2024
Published: April 2, 2024

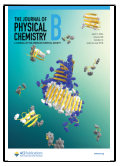

https://doi.org/10.1021/acs.jpcb.3c07176
J. Phys. Chem. B 2024, 128, 3383−3397

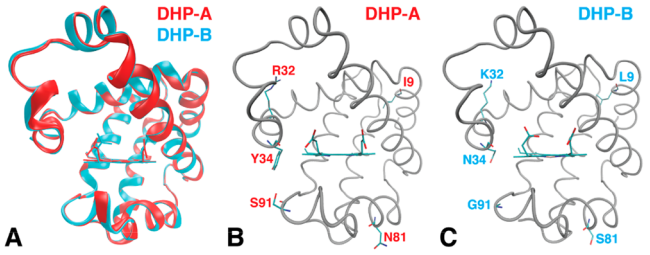

Figure 1. (A) Overlay of DHP-A and DHP-B, (B) DHP-A with its five different amino acids highlighted, and (C) DHP-B with its five different amino acids highlighted (PDB 2QFK, 3IXF).

2,4,6-trichlorophenol (TCP), horseradish peroxidase (HRP) has a rate constant of $k_1 \approx 10^6\ s^{-1}$ for the heterolytic cleavage of H_2O_2, while these rate constants are on the order of $k_1 \approx 10^4\ s^{-1}$ for both DHP-A and DHP-B.[18,19] The rate constants in the peroxidase scheme are listed in Figure 2. The primary difference in activity between DHP-A and DHP-B is in the electron transfer rate constants, k_2 and k_3. However, X-ray crystal structures and enzymatic studies show that both DHP isoenzymes cocrystallize with the same substrates in similar ways and that they oxidize peroxidase substrates by the same mechanism. Although the mechanism of the DHP functional switch is not currently resolved, a standing hypothesis suggests that the chemical class of the substrate dictates enzyme function. For example, phenols are well-known peroxidase substrates in a wide range of peroxidases, and it has been shown that DHP is able to switch from an oxygen-binding to a peroxidase function using phenol binding as a trigger.[20] DHP-B also has much greater peroxygenase activity than DHP-A. DHP-B oxidizes indoles via a peroxygenase mechanism, while other substrates, such as cresols, can be oxidized sequentially via both peroxidase and peroxygenase mechanisms.[9,11] Several spectroscopic studies have been employed to investigate this phenomenon, but the results lead to a structure−function conundrum because of ambiguity in the substrate-binding site.

The site of substrate binding in solution is still in question and may differ substantially from the observed binding in crystals. While X-ray structures show substrates exclusively binding inside the distal pocket, there is evidence for the possibility of both internal and external binding occurring in solution.[16,21−23] We still do not know how much of the chemistry can occur for substrates internalized in the distal cavity of the globin, which is now identifiable as a substrate binding site.[11,18,24−26] Various DHP mutants have been studied to probe the effects of electrostatics and dynamics on substrate binding. Electrostatic mutants that increase the negative charge on the surface of DHP-A have revealed a significant decrease in the rate for oxidation of TCP, which is also negatively charged at pH 7.[27] This raises the question of how the negatively charged substrate enters the hydrophobic distal pocket in wild-type DHP. Effects of site mutations on the distal (His55) and proximal (His89) ligands have been investigated, and all mutations result in a significant decrease and in some cases a complete loss of enzymatic activity.[5,28] Mutations on the proximal side, near His89, designed to increase the polarization of the charge relay decreased the activity instead of making DHP more like a traditional peroxidase.[29] These chemical changes reveal fine-tuning of the heme Fe active site and accessibility of the substrate (or inhibitor) to the distal cavity. Dynamic effects are evident in mutations on neighboring residue Thr56. Smaller amino acids in this position that increase the flexibility of His55 have been shown to improve the catalytic rate constant by providing access to other conformational states unavailable on wild-type DHP.[30] Conversely, Thr56 mutations with bulkier side chains decrease His55 flexibility and catalytic activity. These studies suggest that X-ray crystal structures are confined to a restricted conformational space.

The origin of the differences in catalytic efficiencies between the isoenzymes is still uncertain despite an extensive study that investigated the individual and combined effects of the five differing amino acids totaling 22 possible mutant combinations.[31] This study identified the I9L mutation on DHP-A as the only single-point mutation capable of increasing its

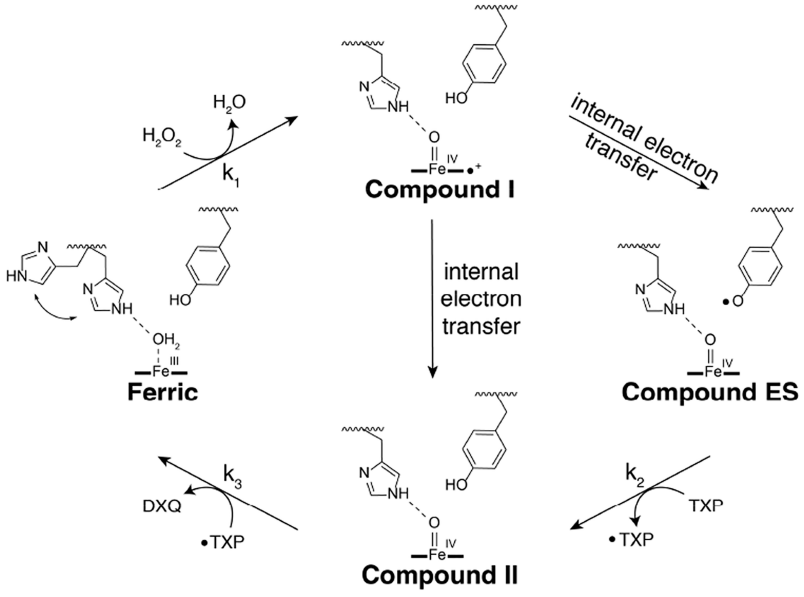

Figure 2. Generic peroxidase reaction scheme of DHP with a trihalophenol (TXP) substrate.

https://doi.org/10.1021/acs.jpcb.3c07176
J. Phys. Chem. B 2024, 128, 3383−3397

catalytic turnover rates similarly to those observed in DHP-B. This observation was surprising because residue 9 is located in a hydrophobic region of the protein more than 15 Å away from the heme iron, and the I9L mutation is quite conservative. This observation led to the hypothesis that differences in conformational dynamics could be responsible for the differences in the reactivity between the two isozymes. Stopped-flow UV−visible spectroscopy and freeze-quench electron paramagnetic resonance (EPR) have provided information on the reactive intermediates in the peroxidase reaction scheme (Figure 2) for both enzymes. The latter studies have shown that the initially formed compound I species rapidly oxidizes one of the five (DHP-A) or four (DHP-B) tyrosine residues.[32,33] Tyr34, present only in DHP-A, is known to play an important role in the formation of compound ES in DHP-A at pH 7, while in DHP-B due to the absence of a tyrosine at position 34, the tyrosyl radical is initially located on Tyr38.[32,34] However, at pH 5, migration of the tyrosyl radical to Tyr38 has been observed in DHP-A. Radical migration also occurs at pH 7 but is significantly slower. A previous enzyme kinetic study suggested that a lower heme and folding stability in DHP-B could be responsible for its higher catalytic efficiency due to a more dynamic structure enabling a higher substrate uptake.[17] Dissociation constants for the important substrates 2,4-dichlorophenol and TCP are both 5 times smaller in DHP-B than in DHP-A.[18]

Protein dynamic processes such as allostery, conformational changes, and catalytic turnover take place on a range of different time scales, anywhere from fs to hours and in some cases up to days or even longer.[35−45] Nuclear magnetic resonance (NMR) spectroscopy is a versatile technique that can provide information about a protein's structure and dynamic behavior at an atomic level over a wide range of time scales by measuring the relaxation rates of individual nuclei. In the study presented in this article, the measurable parameters are T_1, T_2, and the steady-state NOEs of each backbone amide group. These NMR experiments can probe motions in the ps−ns range, and in some cases, they can help identify residues undergoing slower motions in the μs−ms time regime. Motions on a faster time scale can provide information about the rate and amplitude of internal motions relative to protein tumbling, while motions in the slower range can provide information about the population of different conformational states due to chemical exchange. NMR studies of conformational dynamics have been used to study the dynamics of oxygen capture by red blood cells, the dynamics of heme axial ligands, and even how differences in flexibility between the deoxy and carbonmonoxy forms of hemoglobin affect conformational exchange processes and allosteric pathways.[46−49] We hope that a similar approach will bring similar insight into the structure−function conundrum of DHP as well as the difference in catalytic efficiencies of its isoenzymes.

Prior to this study, only DHP-A had been studied by utilizing NMR spectroscopy.[22,50,51] Previous one-dimensional NMR studies using paramagnetic shifts in the metcyano form Fe(III)CN provided an overall description of this isoenzyme in the presence and absence of substrates and inhibitors. Its backbone relaxation dynamics were also studied by means of the model-free analysis, providing a general dynamic picture of the backbone flexibility, internal motions, and rates of chemical exchange in DHP-A.[51] The objective of this comparative NMR dynamics study is to complement the DHP-A findings with insights from DHP-B and capture the full dynamic picture of both DHP isozymes.

2. MATERIALS AND METHODS

2.1. Protein Expression, Labeling, and Purification. The following protocol was developed using an $^{15}N/^{13}C$ isotope uniform labeling protocol and previously established DHP expression and purification protocols.[22,52,53] The pET-16b plasmid containing the 6xHis-tag DHP gene was freshly transformed into chemically competent BL21-(DE3) *E. coli* cells. The cells were plated onto LB agar plates with 100 μg/mL ampicillin (Amp) and incubated at 37 °C for 16 h. Single colonies were isolated and used to inoculate 5 mL × 24 LB broth starter growths with 100 μg/mL Amp. These were incubated in a shaker for 16 h at 37 °C and 250 rpm. Then 10 mL of starter growths were transferred to 1 L × 12 of uniformly isotopically labeled ^{15}N growth media containing 100 mL M9 minimal media (60 g Na_2HPO_4, 30 g KH_2PO_4, 5 g NaCl, 5 g $^{15}NH_4Cl$ per liter), 10 mL of a trace elements solution (5 g EDTA, 0.83 g $FeCl_3$, 84 mg $ZnCl_2$, 13 mg $CuCl_2$, 10 mg $CoCl_2$, 10 mg H_3BO_3, 1.6 mg $MnCl_2$ per liter, pH 7.5), 2 g D-glucose, 1.2 g $MgSO_4$, 33.3 mg $CaCl_2$, 10 mg biotin, 10 mg thiamine, 100 mg hemin, and 100 mg Amp. For uniformly labeled $^{15}N,^{13}C$ protein D-glucose was substituted for D-glucose-$^{13}C_6$. These cultures were incubated in a shaker for 8 h at 37 °C and 250 rpm. The cells were induced with 1 mL of 750 mM isopropyl β-D-1-thiogalactopyranoside (IPTG) per liter and allowed to incubate for another 12 h at 25 °C and 250 rpm, and then they were collected via centrifugation at 4 °C and a relative centrifugal force (RCF) of 2085 for 30 min. The cell pellet was resuspended in 200 mL lysis buffer (50 mM KP_i, 20 mM imidazole, pH 7.4), 10 mg lysozyme, 2 mg soybean trypsin inhibitor (STI), 15 mg phenylmethylsulfonyl fluoride (PMSF), 2 mg tosyl phenylalanyl chloromethyl ketone (TPCK), and 1 mL Triton X-100. The cell slurry was stirred at 4 °C for 1 h and sonicated using eight cycles of a 3 min 20 kHz wave pulse (1.0/0.5 s) followed by a 5 min delay. Supernatant containing His-tagged DHP was collected via centrifugation at 4 °C and an RCF of 26960 for 30 min. The supernatant was loaded and purified at 4 °C in a Ni-NTA agarose column; washed with a 50 mM KP_i, 20 mM imidazole, 300 mM NaCl, pH 7.4 buffer; and eluted with a 50 mM KP_i, 150 mM imidazole, 300 mM NaCl, pH 7.4 buffer. The isolated protein was oxidized to ferric DHP by excess 100 mM $K_3[Fe(CN)_6]$ followed by dialysis against 10 mM KP_i pH 7. The protein was further purified in a CM-52 cation exchange column using 10 and 50 mM KP_i pH 7 as washing and elution buffers, respectively. Only fractions of purified protein with Rz ≥ 3.5 were utilized for analysis. The Rz value is the ratio of the Soret band absorbance at 406 nm to the aromatic amino acid band at 280 nm.

2.2. NMR Sample Preparation. Ferric DHP was concentrated to 1 mM ($\varepsilon_{407\ nm}$ = 116400 $M^{-1}\cdot cm^{-1}$) and mixed with 10-fold excess KCN to obtain the metcyano form of DHP.[54] This is a paramagnetic six-coordinate low-spin (6cLS) S = 1/2 species that produces less dispersed and broadened resonances than the six-coordinate high-spin (6cHS) S = 5/2 metaquo form of DHP.[22] Samples were loaded into 5 mm matched D_2O Shigemi NMR tubes.

2.3. Instruments and Experimental Parameters. Water suppression was achieved using excitation sculpting with gradients.[55] Assignments of the backbone amide resonance of DHP-B were resolved from HNCO, HNCACB, CBCA-

https://doi.org/10.1021/acs.jpcb.3c07176
J. Phys. Chem. B 2024, 128, 3383−3397

(CO)NH, and $^{1}H-^{15}N$ HSQC spectra acquired at 16.45 T (700 MHz for ^{1}H spins) on a Bruker Avance NEO spectrometer equipped with a TCI cryoprobe.[56−64] The relaxation dynamics experiments of DHP-B were performed at 11.75 T (500 MHz) on a Bruker Avance NEO spectrometer equipped with a CPP BBO Prodigy cryoprobe at 16.45 T on a Bruker Avance III instrument and at 19.97 T (850 MHz) on a Bruker Avance III HD instrument, both equipped with a TCI cryoprobe. The relaxation dynamics of DHP-A were done at 11.75 T on a Bruker Avance III HD equipped with a PATXI probe and the previously mentioned 16.45 T Bruker Avance III and 19.97 T Bruker Avance III HD spectrometers. All spectra were recorded at 298 K in 100 mM KP_i pH 7 buffer with 10% D_2O. The T_1 and T_2 experiments had a 3 s recovery delay and relaxation delays equal to {0.1, 0.2, 0.3, 0.5, 0.7, 0.9, 1.1, 1.4, 1.7} s for the measurement of T_1 and {17, 34, 51, 68, 85, 102, 136, 170} ms for the measurement of T_2. The $\{^{1}H\}-^{15}N$ NOE experiments were recorded with and without ^{1}H saturation with a recovery delay of 10 s.

2.4. NMR Data Processing and Analysis. All spectra were processed using *NMRpipe* and visualized with *NMRFAM-SPARKY*.[65,66] *POKY* software was used to calculate the longitudinal (R_1) and transverse (R_2) relaxation rates, the steady-state NOE values, and their respective error values.[67] The relaxation rates were obtained by fitting a single exponential decay function of the form $I(t) = I_0\, e^{-R_n t}$, where $I(t)$ is the intensity after a delay of time t, I_0 is the initial intensity, and R_n is the relaxation rate (R_1 or R_2). The steady-state NOEs were calculated by the ratio of the average intensities of the peaks with and without ^{1}H saturation. The errors in the relaxation rates were calculated from the covariance matrix, while the errors in the NOEs were determined by using the root-mean-square value of the background noise.

2.5. Model-Free Analysis. The model-free formalism, developed by Lipari and Szabo and later extended by Clore et al., was applied to the relaxation data to extract information about the overall tumbling and internal motions of DHP at different time scales.[68−70] It accomplishes this by optimizing the parameters of the spectral density function using various diffusion models and choosing the best fitted model for each individual $^{1}H-^{15}N$ bond vector. Since the overall protein tumbling and its internal motions occur on different time scales, the global correlation function $C(t)$ can be factored into two correlation functions describing each motion as

$$C(t) = C_O(t)\, C_I(t) \tag{1}$$

$$C_O(t) = \frac{1}{5}\sum_{i=-k}^{k} c_i e^{-t/\tau_i} \tag{2}$$

$$C_I(t) = S^2 + (1 - S^2)e^{-t/\tau_e} \tag{3a}$$

$$\tau^{-1} = \tau_m^{-1} + \tau_e^{-1} \tag{3b}$$

where $C_O(t)$ and $C_I(t)$ are the correlation functions describing the overall protein tumbling and the internal motions of the bond vectors, respectively; c_i and τ_i are the coefficients and correlation times of the exponential terms; S^2 is the generalized order parameter with values in the range of [0, 1] that describes the amplitude of the motion of a H−N bond vector; τ_e is the effective correlation time associated with the rate of the motion of individual bond vectors; and τ_m is the correlation time associated with the overall protein motion.[68,69] When the correlation function $C_I(t)$ fails due to the internal motions having both fast and slow components, the extended model-free model is used instead. In this model, the correlation function is redefined as

$$C_I(t) = S^2 + (1 - S_f^2)e^{-t/\tau_f} + (S_f^2 - S^2)e^{-t/\tau_s} \tag{4a}$$

$$S^2 = S_f^2 S_s^2 \tag{4b}$$

where the faster internal motions (< 200 ps) are described by S_f^2 and τ_f and slower motions are described by S_s^2 and τ_s, with $\tau_f < \tau_s < \tau_m$.[70,71] Spectral density functions $J(\omega)$ are the Fourier transform of the correlation functions, and they represent the probability of finding motions at a given angular frequency ω attributed to the relaxation of ^{15}N in the $^{1}H-^{15}N$ bond vector (or ^{13}C in a $^{1}H-^{13}C$ bond vector).[68,72,73] Thus, the spectral densities evaluated at various frequencies can be used to reconstruct the autocorrelation function of each bond vector to obtain information about internal dynamics. The Fourier transform of eqs 3a and 4a yields the following model-free spectral densities:[74,75]

$$J(\omega) = \frac{2}{5}\sum_{i=-k}^{k} c_i\tau_i\left(\frac{S^2}{1 + (\omega\tau_i)^2} + \frac{(1 - S^2)(\tau_e + \tau_i)\tau_e}{(\tau_e + \tau_i)^2 + (\omega\tau_e\tau_i)^2}\right) \tag{5}$$

$$J(\omega) = \frac{2}{5}\sum_{i=-k}^{k} c_i\tau_i\left(\frac{S^2}{1 + (\omega\tau_i)^2} + \frac{(1 - S_f^2)(\tau_f + \tau_i)\tau_f}{(\tau_f + \tau_i)^2 + (\omega\tau_f\tau_i)^2} + \frac{(S_f^2 - S^2)(\tau_s + \tau_i)\tau_s}{(\tau_s + \tau_i)^2 + (\omega\tau_s\tau_i)^2}\right) \tag{6}$$

An analysis of the relaxation dynamics of DHP was carried out using the extended model-free approach as implemented in the *eMF* (*easy Model Free*) software developed by Sung-Hung Bae.[76] An overall axially symmetric rotational diffusion tensor was optimized using bond vectors with NOE > 0.65, a chemical shift anisotropy value of −172 ppm, and an average amide H−N bond distance of 1.02 Å. The best fitting model for each bond vector was selected by the Akaike information criteria (AIC) after the exclusion of unrealistic models containing $S^2 > 1$, $\tau_e < 0$, or $R_{ex} < 0$, and the error propagation of the model-free parameters were determined by 500 Monte Carlo simulations.

2.6. Molecular Dynamics and Trajectory Analysis. Molecular dynamics (MD) simulations were performed in *NAMD* with the *CHARMM36* additive all-atom force field parameters.[77−96] The carbonmonoxy form of DHP is isoelectronic with metcyano DHP and was used for the simulations since the carbonmonoxy parameters have been more extensively validated and are considered sufficient for the purpose of simulating backbone dynamic motions. As previously mentioned, His55 exhibits allosteric behavior between two conformations: a closed conformation corresponding to a 6cHS heme iron and an open solvent-exposed conformation corresponding to a 5cHS heme iron (Figure 3).[6] In the absence of substrate or ligand, resonance Raman data shows that His55 in metaquo DHP is in equilibrium between the two conformations, with approximately 60% in the closed conformation and 40% in the open conformation.[4] We simulated both His55 conformations to assess their influence

https://doi.org/10.1021/acs.jpcb.3c07176
J. Phys. Chem. B 2024, 128, 3383−3397

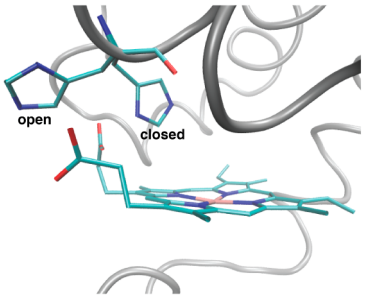

Figure 3. Open and closed conformations of His55 in DHP-B (PDB 3IXF).

on the relaxation dynamics. Models were constructed using X-ray crystal structures of wild-type DHP (PDB 2QFK, 3LB1, and 3IXF) centered and solvated in a unit cell of dimensions 50.5 Å × 57.2 Å × 60.7 Å. The structures were ionized and neutralized by adding K^+ and Cl^- ions to simulate a 100 mM ionic strength solution. This ionic composition was chosen because studies of DHP are normally performed in 100 mM potassium phosphate buffer. Periodic boundary conditions were applied with an interaction cutoff of 12 Å and a force switch smoothing function from 10 to 12 Å. Timesteps were set to 2 fs, and full electrostatic interactions were calculated using the particle mesh Ewald method on every other step.[97] Langevin dynamics with a damping coefficient of 1.0 were applied to all non-hydrogen atoms. Structures were minimized and equilibrated for 5 ns prior to all simulations, and trajectories were analyzed from 300 ns of simulation time. The *carma* software was used to remove global rotational−translational motions from the simulation trajectories.[98] Unit vectors of the backbone amide bond vector were extracted and analyzed by means of the NMR analysis module of *CHARMM* to calculate the bond autocorrelation function of internal motion and square generalized order parameters.[99−101]

3. RESULTS

3.1. Backbone Assignment of Dehaloperoxidase B. Backbone $^{13}C_\alpha$, $^{13}C_\beta$, carbonyl ^{13}C, and amide ^1H and ^{15}N resonances of metcyano DHP-B were assigned from CBCA-(CO)NH, HNCACB, HNCO, and $^1H-^{15}N$ HSQC experiments. A total of 119 out of 137 (87%) backbone residues were assigned. The quality of the $^1H-^{15}N$ HSQC spectrum (Figure 4) shows good peak dispersion with minimal peak overlap. All assigned resonances are presented in Table S.1 along with previously assigned resonances of metcyano DHP-A.

3.2. Relaxation Dynamics. NOE values and relaxation rates of both DHP isoenzymes are presented in Figure 5. A total of 113 residues have assigned resonances in both DHP-A and DHP-B, thus those are the ones that will be compared (Δvalues) in the following sections. Both R_1 and R_2 relaxation rates are generally similar among the isoenzymes, with the exception of Phe35. Overall, both DHP isoenzymes exhibit similar steady-state $\{^1H\}-^{15}N$ NOEs with the lowest values in the EF and GH loop regions, with average values of less than 0.30 and 0.50, respectively. These low NOE values could be due to the bond vectors either partaking in chemical exchange or undergoing motions faster than the overall tumbling of the protein. In DHP-A, the NOE of residue Phe35 could not be measured, and the measurement of its T_2 was challenging, possibly due to chemical exchange. Comparison of the HSQC data at the three magnetic fields in this study provides evidence of a peak splitting that may arise from slow chemical exchange.[102,103] As observed in Figure 10, this effect is more evident at higher fields. Although R_1 is similar for both peaks, R_2 differs considerably, suggesting two conformations with different relaxation rates. This behavior of Phe35 in DHP-A was observed to be anomalous in a previous relaxation dynamics study, but the significance of a slow chemical exchange became evident only at 19.97 T.[51]

3.3. Spectral Densities and Consistency Testing. Experimental relaxation parameters R_1, R_2, and $\{^1H\}-^{15}N$

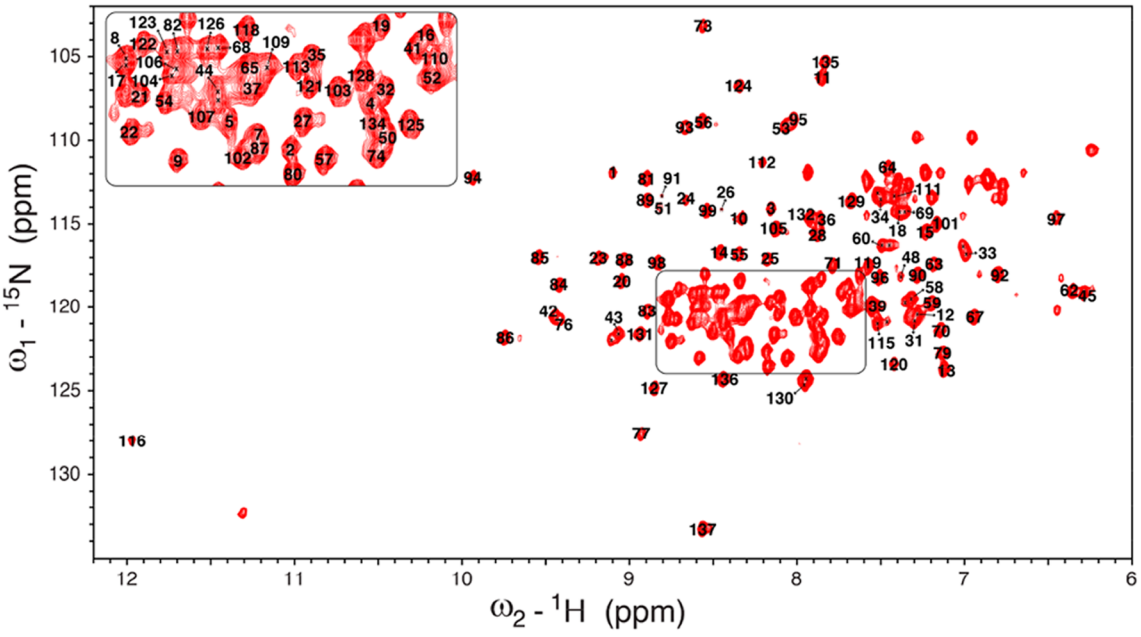

Figure 4. $^1H-^{15}N$ HSQC backbone assignments of metcyano DHP-B in 100 mM KPi, pH 7 with 10% D_2O at 298 K and 16.45 T.

https://doi.org/10.1021/acs.jpcb.3c07176
J. Phys. Chem. B 2024, 128, 3383−3397

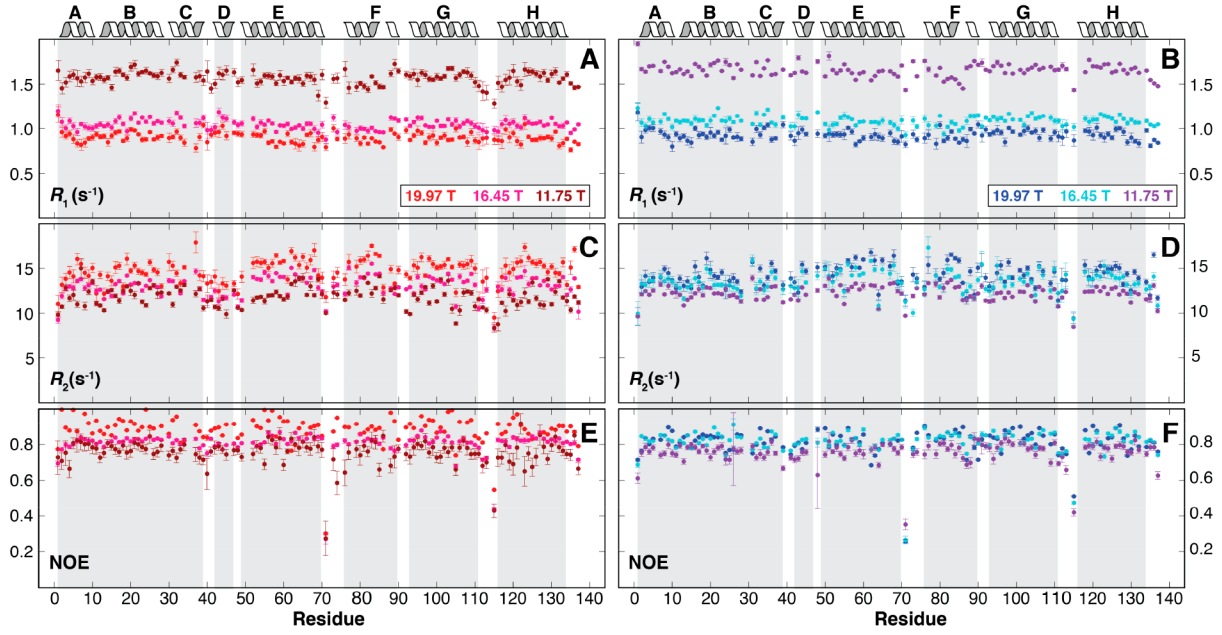

Figure 5. R_1, R_2, and NOE data of DHP-A (left) and DHP-B (right) measured at 11.75, 16.45, and 19.97 T. DHP α-helical regions are shown at the top. (A) R_1 values of DHP-A, (B) R_1 values of DHP-B, (C) R_2 values of DHP-A, (D) R_2 values of DHP-B, (E) NOE values of DHP-A, and (F) NOE values of DHP-B.

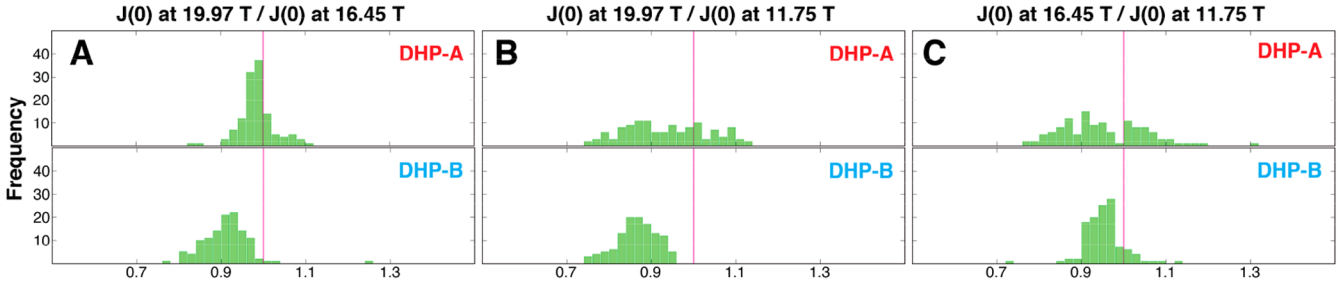

Figure 6. Correlation plots of the calculated $J(0)$ values for the consistency testing of DHP-A and DHP-B between data sets at (A) 19.97 and 16.45 T, (B) 19.97 and 11.75 T, and (C) 16.45 and 11.75 T.

NOE are a direct measurement of the spectral density, $J(\omega)$, and each of these parameters can be expressed as a linear combination of the spectral densities $J(0)$, $J(\omega_H)$, $J(\omega_N)$, and $J(\omega_H \pm \omega_N)$.[68,104,105] Small variations in instruments, sample acquisition, and conditions can introduce artifacts that result in inconsistent relaxation data collected in different magnets and magnetic fields, providing an incorrect characterization of the dynamics in the model-free analysis.[106] Consistency between data sets can be verified by calculating the spectral density of every bond vector at the zero frequency, which is independent of the magnetic field. Correlation of the $J(0)$ values at different magnetic fields is shown in Figure 6. The consistency tests for DHP-A show that the relaxation data at 19.97 and 16.45 T are consistent with each other but not with the data at 11.75 T. Therefore, the latter were not included in the model-free analysis for this isoenzyme. It is possible that data obtained at 11.75 T for DHP-A are inconsistent with the other two fields because the magnet used was not equipped with a cryoprobe like the others. All magnets used for measuring DHP-B dynamics were equipped with cryoprobes. Consistency tests for DHP-B showed that all data sets are consistent with each other, but their values shift in a field-dependent manner. The shift could be caused by slow motions in the μs−ms time regime like chemical exchange, which are known to affect R_2 in this manner.[105−109] All data sets of DHP-B were used in the model-free analysis.

3.4. Model-Free Analysis. Prior to application of the model-free analysis, the T_1/T_2 ratio was used to estimate τ_m and the generalized order parameter for each bond vector as a final data quality check. This can help identify spins that might be exchange broadened and result in unrealistic S^2 values, which could prevent the model-free analysis from converging.[110−112] The estimated τ_m and theoretical S^2 values at all magnetic fields are shown in Figure 7, where the values of τ_m increase clockwise along each curve (starting at the bottom right). Most residues were estimated to have reasonable S^2 values, except Phe123 in DHP-A at 19.97 T and Lys51 in DHP-B at 11.75 T. These two minor violations notwithstanding, no spins were omitted from the model-free analysis.

Parameters obtained from the model-free analysis are shown in Figure 8. Differences in the overall tumbling correlation times of the two isoenzymes are negligible, with τ_m values of 9.52 ± 0.01 and 9.50 ± 0.01 ns for DHP-A and DHP-B, respectively. Additionally, the average S^2 values show that both isoenzymes have similar overall flexibility, with an average value of 0.84 ± 0.02 in DHP-A and 0.85 ± 0.02 in DHP-B. For

https://doi.org/10.1021/acs.jpcb.3c07176
J. Phys. Chem. B 2024, 128, 3383−3397

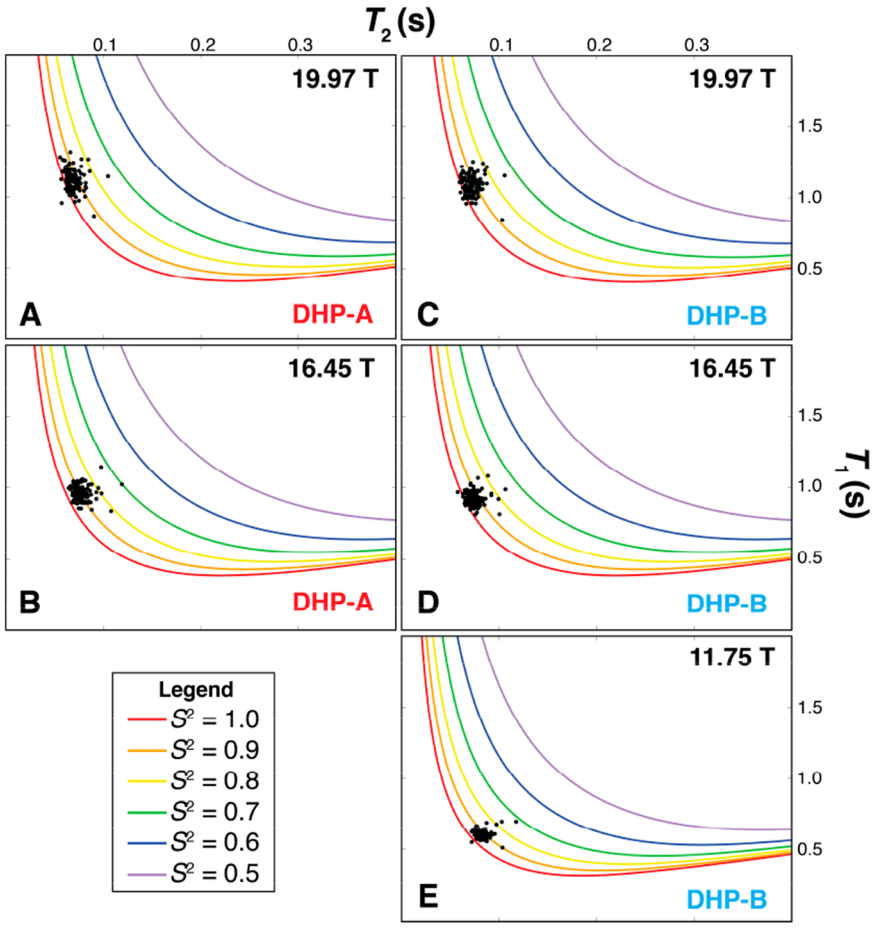

Figure 7. Experimentally determined T_1 vs T_2 for 1 mM DHP isoenzymes overlaid with predicted model-free values of S^2 order parameter values. Predicted S^2 from experimental data of DHP-A at (A) 19.97 T and (B) 16.45 T and for DHP-B at (C) 19.97 T, (D) 16.45 T, and (E) 11.75 T.

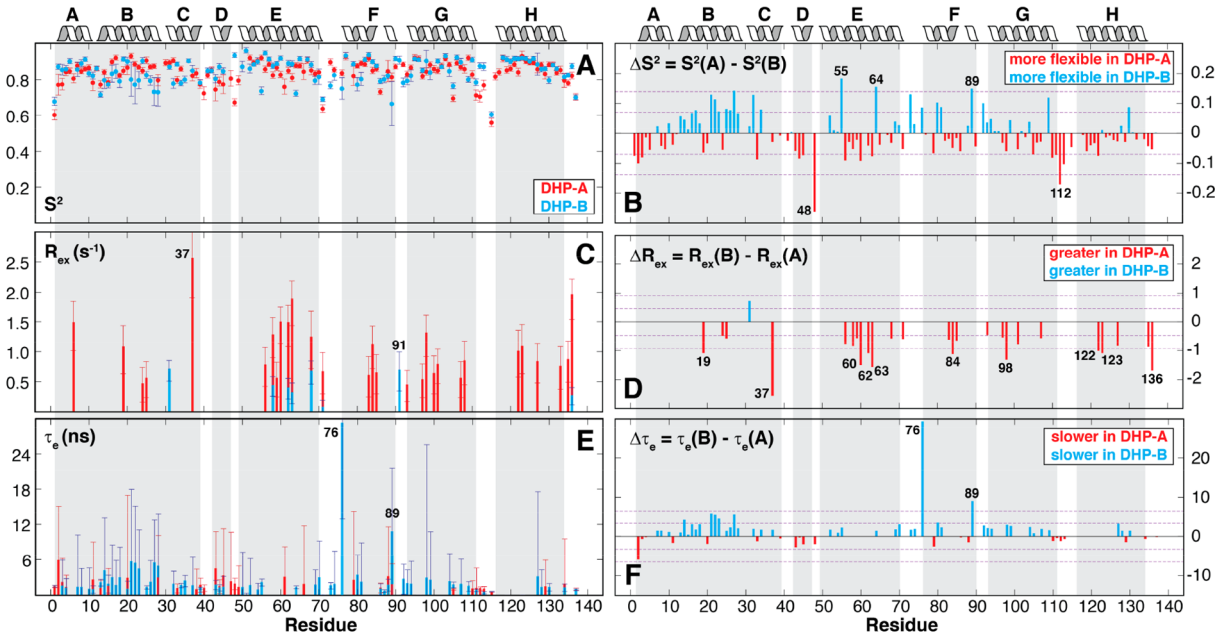

Figure 8. Comparison of NMR relaxation parameters between DHP-A and DHP-B obtained from the model-free analysis. (A) Generalized order parameter S^2, (B) differences in S^2 values, (C) rate of chemical exchange R_{ex}, (D) differences in R_{ex} values, (E) effective correlation times τ_e, and (F) differences in τ_e values. Values of $\pm 2\sigma$ and $\pm 1\sigma$ are represented by purple dashed lines in panels B, D, and F.

https://doi.org/10.1021/acs.jpcb.3c07176
J. Phys. Chem. B 2024, 128, 3383−3397

a residue-to-residue comparison of all relaxation parameters, values with a difference greater than 2σ are considered significant. The lowest S^2 values in both isoenzymes were located in the GH loop region, where the lowest NOE values were also observed. S^2 is inversely proportional to a spherical cone of motion accessible to the amide (N═H) bond vector. $S^2 = 1$ would mean the N−H bond vector has a unique projection and is rigid, and $S^2 = 0$ means that the vector can access the entire sphere. The term flexibility is used to qualitatively describe the change in ΔS^2. The most significant ΔS^2 ($2\sigma = 0.14$) was observed in Ser48, where the S^2 value was 0.26 smaller in DHP-A. This 26% decrease in S^2 indicates that Ser48 exhibits a greater flexibility in DHP-A. The second most significant ΔS^2 was observed at His55 (distal histidine) which was 18% smaller in DHP-B. All other residues with significant ΔS^2 are highlighted in Figure 8B. From these, we bring attention to His89 (proximal histidine) which had a 15% smaller S^2 in DHP-B. This shows that both distal and proximal histidines, key residues in the peroxidase catalytic cycle of DHP, are significantly more flexible in DHP-B. In contrast to DHP-B, many residues in DHP-A appear to undergo chemical exchange. Due to the identical experimental conditions, these differences were attributed to differences in conformational dynamics between the isoenzymes. The most significant difference in the rate of chemical exchange, ΔR_{ex} ($2\sigma = 0.93$), was observed in Asn37. It had an R_{ex} of 2.56 s^{-1} in DHP-A, but it did not undergo chemical exchange in DHP-B. This was the largest chemical exchange rate observed in either isoenzyme. In contrast, the largest R_{ex} observed in DHP-B was in Glu31 with 0.71 s^{-1}. Additionally, Gly91 in DHP-B, one of the five differing residues between the isoenzymes, has an R_{ex} term, but the corresponding Ser91 in DHP-A has no assigned resonance; thus, a comparison between the two is not possible. None of the other four differing residues appear to undergo chemical exchange in either isoenzyme. The effective correlation times (τ_e) show that more bond vectors undergo slower motions in DHP-B than in DHP-A. Most notably, Leu76 has a τ_e of 29 ns in DHP-B, meaning that its motion is about 3 times slower than the overall tumbling motion of DHP-B. This residue is located at the terminus of α-helix F in the dimer interface. The other residue with significant $\Delta\tau_e$ ($2\sigma = 6.5$) is His89, which is ∼9 ns slower in DHP-B than in DHP-A. Since His89 was predicted to be 15% more flexible in DHP-B, the observations correspond to a simultaneous greater range of but slower motion of this residue in DHP-B. These observations may be related to the fact that DHP-B has a lower folding stability than DHP-A and heme loss is the first step in protein unfolding.[17]

3.5. MD Simulations. The generalized order parameter can also be approximated from MD trajectories by removing the overall translational and rotational motions of the protein and obtaining the correlation function for each bond vector. The motions were removed by fixing the C_α positions in a reference frame and superimposing and aligning the trajectory. In the NMR analysis module of *CHARMM*, the spectral density is defined as

$$J_n(\omega) = \int_0^\infty \langle Y_n^2(\theta(t)\phi(t)) \cdot Y_n^{2*}(\theta(0)\phi(0)) \rangle \cos(\omega t)\, dt \tag{7}$$

where $Y_n^2(\theta(t)\phi(t))$ are second-order spherical harmonics and the angular brackets are the internal correlation function of the n^{th} bond vector.[104,113] The spectral density can be simplified to

$$J(\omega) = \int_0^\infty C_I(t) \cos(\omega t)\, dt \tag{8}$$

with the internal correlation function and the generalized order parameter defined as

$$C_I(t) = A\langle P_2[\mu(t) \cdot \mu(t + t')] \rangle \tag{9}$$

$$S^2 = \lim_{t \to \infty} C_I(t) \tag{10}$$

where P_2 is the second Legendre polynomial and $\mu(t)$ and $\mu(t + t')$ are unit vectors corresponding to the orientation of the bond vector at times t and $t + t'$ over the trajectory and the generalized order parameter is approximated from the convergence of the correlation function.[114,115]

The S^2 parameters calculated from 300 ns MD trajectories are shown in Figure 9 for the two allosteric isomers of His55 in each isoenzyme. The allosteric behavior of His55 has been observed by X-ray crystallography, and it depends on conditions of ligation and inhibitor or substrate binding.[3] The closed conformation ($His55_{in}$) consists of His55 positioned inside the distal pocket within the hydrogen bonding distance of bound ligands such as O_2, F^-, and CN^-.[24,116,117] The open conformation ($His55_{out}$) consists of His55 in a solvent-exposed position, and it is observed in the deoxy heme and, surprisingly, in the CO structure of DHP-A.[3,6] Since the time required for conversion from one conformation to the other is beyond the MD simulation

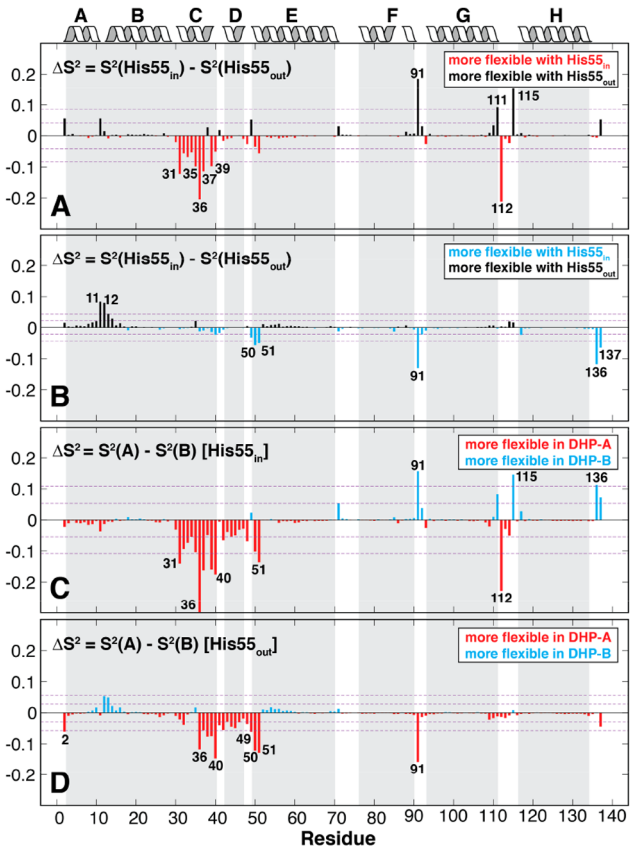

Figure 9. Effects of the allosteric behavior of His55 on S^2 values in both DHP-A and DHP-B determined from 300 ns MD trajectories. (A) Effects of the His55 conformation in DHP-A, (B) effects of the His55 conformation in DHP-B, (C) effects of $His55_{in}$ in both DHP isoenzymes, and (D) effects of $His55_{out}$ in both DHP isoenzymes.

https://doi.org/10.1021/acs.jpcb.3c07176
J. Phys. Chem. B 2024, 128, 3383−3397

time scale, both conformations were studied separately to obtain a complete understanding of the relevant conformational space. Simulations predict that the orientation of His55 has a greater impact on the S^2 values in DHP-A than in DHP-B. The three most significantly affected residues ($2\sigma = 0.08$) by the His55 orientation in DHP-A were Gly112, Lys36, and Ser91 with changes in S^2 of 19−21%. Additionally, a majority of residues in α-helix C (residues 29−39) were significantly affected, and the closed conformation of His55 causes a decrease in S^2 in that region of 10−20%. In DHP-B, the three most significantly affected residues ($2\sigma = 0.04$) are Gly91, Met136, and Gly11 with their S^2 values changing by 8−13%. Comparing the two DHP isoenzymes, the α-helix C region is the most different and it is more flexible in DHP-A regardless of the orientation of His55.

The largest difference by far in interisozyme dynamics was observed at residue Phe35. The adjacent amino acid at position 34 is asparagine in DHP-B and the primary tyrosyl radical site in DHP-A at pH 7. At higher field, the Phe35 resonance appears to be a double peak in DHP-A. A single broadened peak is observable at 11.75 T, but a splitting into two peaks is increasingly distinguishable at 16.45 and 19.97 T as shown in Figure 10. This splitting indicates that Phe35 is in

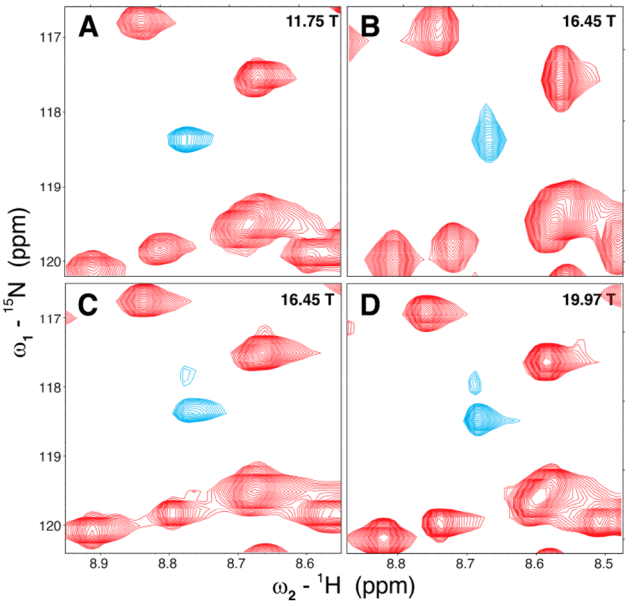

Figure 10. HSQC spectra of DHP-A showing Phe35 (resonance in blue) recorded at different fields. (A) Spectrum recorded at 11.75 T, (B and C) spectra recorded at 16.45 T, and (D) spectrum recorded at 19.97 T. Panel C shows data collected in our previous dynamics study.[51]

slow chemical exchange between two conformational states, Phe35κ_1 and Phe35κ_2, in DHP-A. The T_1 and T_2 decays of both states at 16.45 and 19.97 T are shown in Figure S1. Relaxation rates of Phe35 in both isoenzymes are summarized in Table 1. The two conformations of Phe35 in DHP-A have R_1 rates comparable to those observed in DHP-B. However, the R_2 rates show that the Phe35κ_2 conformation relaxes about an order of magnitude slower in comparison to Phe35 in DHP-B, while the Phe35κ_1 conformation relaxes so rapidly that the rate could not be reliably fitted to an exponential function.

Table 1. Relaxation Rates of Phe35 in DHP-A and DHP-B at 16.45 and 19.97 T

B_0 (T)	State		R_1 (s^{-1})	R_2 (s^{-1})
16.45	DHP-A	κ_1	1.47 ± 0.35	[a]
		κ_2	1.27 ± 0.31	1.19 ± 0.44
	DHP-B	-	1.21 ± 0.02	12.95 ± 0.47
19.97	DHP-A	κ_1	0.90 ± 0.26	[a]
		κ_2	0.87 ± 0.25	1.05 ± 0.44
	DHP-B	-	1.04 ± 0.02	13.98 ± 0.29

[a]Fitting not possible.

4. DISCUSSION

The results of relaxation dynamics experiments show relatively few areas of difference in the protein dynamics of DHP-A and DHP-B. This is not surprising given the overall structural similarity of the two isozymes. However, there are a few important differences in order parameters, which report on the relative freedom of motion of amide bonds. The largest difference is in residue Ser48 with a 26% smaller S^2 in DHP-A, and its value of 0.672 ± 0.020 is indicative of a relatively disordered residue. Ser48 is located on the surface of DHP in the DE turn region. Next are His55, Met64, and His89 with 15−18% smaller S^2 values, indicating greater flexibilities in DHP-B. On the other hand, MD simulations predicted that the α-helix C region (residues 29−39) is where the dynamics of the two isoenzymes significantly differ. This entire region is predicted to have lower S^2 values in DHP-A, especially residue Lys36, with a 31% smaller value. A complete listing of R_1, R_2, NOE, and S^2 values calculated from NMR and MD simulations is provided in Tables S.2−S.5.

4.1. Effects of Chemical Exchange. The two isozymes have a systemic difference in their chemical exchange rates. A total of 23% of the assigned residues in DHP-A have an R_{ex} term, while only 7% do in DHP-B. Additionally, the average exchange rate in DHP-A is 2.3-fold greater than in DHP-B, and the largest rate was observed in Asn37 in DHP-A. Finally, there is a significant difference in the relaxation of Phe35 that is attributed to the presence of slow chemical exchange in DHP-A. These findings are likely to be important for the enzyme function given (1) the proximity of Phe35 to residue 34, which is Tyr34 in DHP-A and Asn34 in DHP-B, as well as (2) the proximity of Asn37 to Tyr38 in both enzymes. This is because the formation of tyrosine radicals plays a major role in the deactivation and cross-linking pathways that compete with the enzymatic reactivity in DHP.

In proteins, chemical exchange often involves relatively slow processes such as conformational fluctuations, dimerization, and even substrate binding.[107,118] For example, there is evidence of a dynamic dimerization equilibrium of DHP in solution. Although DHP is known to exclusively crystallize as a dimer, a SAXS study showed that it is approximately 10% dimeric in solution.[119] In X-ray crystal structures, the dimer interface is observed between the α-helix H of one monomer subunit and the EF loop region of the other, involving residues Tyr71, Asp72, Arg122, and Asn126.[120] This region is where the lowest NOE values were observed for both isoenzymes; thus, it is reasonable to propose that these are a consequence of transient dimerization in solution since low NOE values are typically observed in the presence of rapid motions or chemical exchange. Chemical exchange cannot be directly measured from NOE or relaxation rates; however, it can be observed indirectly owing to a shortening of T_2.[102,107,118]

https://doi.org/10.1021/acs.jpcb.3c07176
J. Phys. Chem. B 2024, 128, 3383−3397

Both NMR dynamics data and MD simulations show that chemical exchange is important in Phe35 in DHP-A despite the fact that the available DHP-A and DHP-B X-ray structures showed Phe35 in a single conformation (Figure 11).

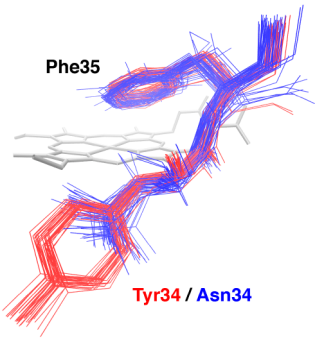

Figure 11. Overlay of all available X-ray structures DHP-A (red) and DHP-B (blue) with a focus on residue 34 and Phe35.

Nonetheless, measurement of the Phe35 C_α–Fe distance over the 300 ns MD trajectories in DHP-A (Figures S.2 and S.3) supports the hypothesis that Phe35 has two conformations but only when His55 is in the closed conformation. The two conformations have Phe35 C_α distances of approximately 9.1 and 10.4 Å away from the heme iron. Extracted structures from the MD trajectories (Figure 12) show that the increase in

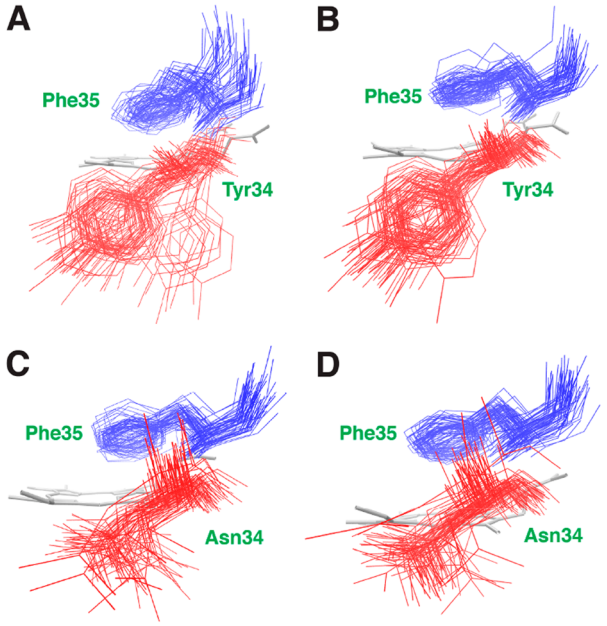

Figure 12. Conformations of residue 34 (red) and Phe35 (blue) from every 10000th frame of the 300 ns MD trajectory of (A) DHP-A with $His55_{in}$, (B) DHP-A with $His55_{out}$, (C) DHP-B with $His55_{in}$, and (D) DHP-B with $His55_{out}$.

the Phe35 C_α–Fe distance is caused by a *swinging* motion in Tyr34 that causes its C_α to push the C_α and side chain of Phe35 toward the inside of the distal pocket. These motions are mainly coupled through the backbone. This secondary structure of Phe35 is not observed in DHP-A when His55 is in the open conformation or in DHP-B with either His55 conformation. In DHP-B, the average Phe35 C_α–Fe distance is 9.0 Å. Moreover, DHP-B Asn34 is in the same position as the DHP-A Tyr34 conformation, which does not displace Phe35 (Figure 12B). It appears that Tyr34 might have a swinging motion in solution, which is not observed in X-ray structures due to crystal packing limitations (Figure 11). The NMR dynamics data reveal motions in DHP that are not evident in X-ray structures, as observed in other proteins, such as the flap dynamics observed in HIV-1 protease and the allosteric cooperativity network in the catalytic subunit of protein kinase A.[121−123]

His55 exists in a 60:40 equilibrium between its closed and open conformations when water is bound to the heme iron. A resonance Raman study showed that His55 adopts an open conformation upon binding of parahalogenated phenols (inhibitors) in the distal pocket, while trihalogenated phenols (substrates) cause it to adopt a closed conformation.[21] The NMR samples contain metcyano DHP with CN^- bound to the heme iron, and it is therefore likely that His55 is in the closed conformation as observed in X-ray crystal structures.[116] Consequently, the experimentally observed slow chemical exchange at Phe35 could be due to the Tyr34/Phe35 conformational states seen in the MD simulations. Experimental S^2 values show that Tyr34 in DHP-A has an 8% greater value than the corresponding Asn34 in DHP-B. Moreover, Tyr34 has a more rigid side chain than Asn34, which could explain the coupling of its motion to Phe35. Asn37 in DHP-A also had the largest R_{ex} (2.6 s^{-1}) of any residue in either isoenzyme. There is no R_{ex} term associated with Asn37 in DHP-B, meaning that this residue undergoes fast chemical exchange in DHP-A relative to that in DHP-B. Asn37 is adjacent to Tyr38, the primary tyrosyl radical in DHP-B at both pH 7 and 5 and in DHP-A at pH 5.[32,34] It is possible that the fast chemical exchange of Asn37 could interfere with the tyrosyl radical formation at Tyr38 in DHP-A at pH 7, which is the pH studied in this work. MD simulations also showed the greatest ΔS^2 at Lys36, which is estimated to be 31% smaller in DHP-A. Unfortunately, there is no assignment of Lys36 in DHP-A to make a comparison with experimental data. These observations suggest that the region between the functionally important Tyr34 and Tyr38 could be involved in conformational changes in DHP-A that negatively impact the tyrosyl radical formation with a concomitant decrease in catalytic efficiency.

4.2. S^2 Order Parameters at Key Sites. Generalized order parameters of the five differing residues in DHP-A and DHP-B and flanking residues are listed in Table 2. Only four of the five differing amino acids can be compared because Ser91 in DHP-A has no assigned resonance. The greatest ΔS^2 was observed at R32K followed by Ala80 and N81S with values 9–13% smaller in DHP-B; however, these differences are within the 2σ region for changes in S^2 (2σ = 0.14) and are not considered to be significant. In a previous mutational study of DHP-A, the I9L mutation was identified as the only one capable of increasing the catalytic turnover to rates similar to those observed in DHP-B.[31] Despite its pivotal role in the difference in reactivity between the isoenzymes, neither the X-ray structures nor the NMR dynamics experiments have elucidated the reasons for the effect of the I9L substitution on catalytic turnover rates. There are also no significant dynamics in the region surrounding Tyr38 in DHP-B in any way comparable to the rapid chemical exchange of Asn37 in DHP-A. This chemical exchange could impact the tyrosyl radical formation at Tyr38 in DHP-A, which may explain why Tyr34 is the favored radical site at pH 7. Tyr34 is believed to play an

https://doi.org/10.1021/acs.jpcb.3c07176
J. Phys. Chem. B 2024, 128, 3383−3397

Table 2. S^2 Order Parameters of Differing Residues in the DHP Isoenzymes and Their Neighboring Residues[a]

Residue		S^2_{DHP-A}	S^2_{DHP-B}	ΔS^2
8	Thr	0.846 ± 0.016	0.888 ± 0.020	−0.042
9	**Ile/Leu**	0.858 ± 0.014	0.911 ± 0.012	**−0.053**
10	Arg	0.865 ± 0.015	0.833 ± 0.019	0.032
31	Glu	0.893 ± 0.014	0.871 ± 0.016	0.022
32	**Arg/Lys**	0.905 ± 0.013	0.777 ± 0.027	**0.128**
33	Arg	0.797 ± 0.019	0.884 ± 0.011	−0.087
34	**Tyr/Asn**	0.858 ± 0.014	0.779 ± 0.015	**0.079**
35	Phe	[c]	0.799 ± 0.018	[c]
80	Ala	0.875 ± 0.013	0.772 ± 0.037	0.103
81	**Asn/Ser**	0.889 ± 0.014	0.802 ± 0.036	**0.087**
82	Thr	0.884 ± 0.014	0.909 ± 0.012	−0.025
90	Ser	0.871 ± 0.014	0.915 ± 0.012	−0.044
91	**Ser/Gly**	[b]	0.906 ± 0.022	[c]
92	Leu	0.882 ± 0.013	0.782 ± 0.025	0.100

[a]Differing residues are highlighted in bold. ΔS^2 is defined as $S^2_{DHP-A} - S^2_{DHP-B}$. [b]Assignment not available. [c]Data not available.

important role in the formation of compound ES, which can decay into an inactive ferric species called compound RH.[124] The structure of compound RH is not known, but it is a ferric species believed to involve a protein cross-link similar to those observed in myoglobin and cytochrome *c* peroxidase.[34,124,125] These two crucial tyrosine radical intermediates play a significant role in differences in substrate oxidation kinetics via a peroxidase mechanism in DHP isozymes. There is unfortunately no assigned resonance for Tyr38 on DHP-B for a direct comparison with DHP-A.

Finally, the NMR dynamics inform on the function of the crucial conserved histidines found in both isozymes, the distal histidine (His55) and the proximal histidine (His89) presented in Table 3. In an X-ray crystallographic study, it

Table 3. S^2 Order Parameters of Key Residues in DHP Isoenzymes and Their Neighboring Residues[a]

Residue		S^2_{DHP-A}	S^2_{DHP-B}	ΔS^2
54	Asp	0.904 ± 0.014	0.900 ± 0.018	0.004
55	**His**	0.919 ± 0.015	0.736 ± 0.021	**0.183**
56	Thr	0.856 ± 0.018	0.946 ± 0.011	−0.09
88	Gln	0.845 ± 0.059	0.821 ± 0.017	0.024
89	**His**	0.813 ± 0.022	0.664 ± 0.123	**0.149**
90	Ser	0.871 ± 0.014	0.915 ± 0.012	−0.044
37	Asn	0.820 ± 0.029	0.849 ± 0.028	−0.029
38	**Tyr**	0.834 ± 0.026	[b]	[c]
39	Val	0.773 ± 0.023	0.781 ± 0.017	−0.008
47	Lys	0.805 ± 0.043	[b]	[c]
48	**Ser**	0.672 ± 0.020	0.933 ± 0.013	**−0.261**
49	Met	0.794 ± 0.025	[b]	[c]

[a]Key residues are highlighted in bold. ΔS^2 is defined as $S^2_{DHP-A} - S^2_{DHP-B}$. [b]Assignment not available. [c]Data not available.

was proposed that the S91G substitution in DHP (Ser91 in DHP-A and Gly91 in DHP-B) could increase the flexibility of the proximal histidine in DHP-B because its His89−Fe bond is 0.07 Å longer.[120] The proximal histidine is the axial ligand to the heme iron, which is bonded through the lone pair of nitrogens at Nε. Therefore, the Nε−Fe bond plays an important role in the heterolytic O−O bond cleavage needed for the formation of compound I in DHP. This bond cleavage is accomplished by a classical peroxidase push−pull Poulos-Kraut mechanism, where the distal ligand provides the pull and the proximal ligand provides the push.[126] Although we cannot directly compare the differences in S91G because of the missing assignment of Ser91 in DHP-A, the experimental results show that His89 has a 15% smaller S^2 value in DHP-B. Its value of 0.664 ± 0.123 suggests that the proximal histidine is relatively disordered in DHP-B, supporting the previously proposed higher flexibility of His89 in DHP-B as a result of the S91G substitution. The distal histidine also has an 18% smaller S^2 value in DHP-B, indicative of a higher flexibility in DHP-B. The observed greater flexibility on both distal and proximal ligands in DHP-B is consistent with this isoenzyme's higher catalytic efficiency. Besides providing the pull necessary for the O−O bond cleavage, the allosteric behavior of His55 (closed vs open) is responsible for facilitating the entrance and exit of small molecules into the distal cavity.[5,30] An increase in flexibility should allow more rapid access of substrate molecules into the distal pocket, which would result in an increase in their oxidation rate. This higher flexibility is also consistent with a comparative folding study that revealed that DHP-B has a lower folding stability than DHP-A.[17] This greater range of motion of the DHP-B active site is important in an enzyme that admits many different substrates into its distal pocket.

5. CONCLUSIONS

We assigned a total of 119 out of 137 (87%) backbone resonances of metcyano DHP-B and provided a detailed comparison of the backbone relaxation dynamics of the two DHP isoenzymes at three magnetic fields in combination with four 300 ns MD trajectories. Results show that the isoenzymes have an overall similar backbone flexibility and that in contrast to DHP-B, many residues in DHP-A appear to exhibit chemical exchange. Chemical exchange plays a key role in residues Phe35 and Asn37. In particular, Phe35, which is a neighbor of the Y34N substitution, appears to have two conformational states, namely, Phe35κ_1 and Phe35κ_2. The conformational state Phe35κ_1 has an extremely rapid relaxation, while Phe35κ_2 relaxes about an order of magnitude slower than Phe35 in DHP-B. MD simulations predict that these two conformational states could be a result of a swinging motion in Tyr34 present only when His55 is in a closed position. This motion, coupled only through the backbone, causes the C_α of Tyr34 to push the C_α and side chain of Phe35 upward and toward the distal cavity (or vice versa). Since Tyr34 is known to be the primary tyrosyl radical site in DHP-A at pH 7, it is possible that the presence of these conformational states interferes with the formation of compound ES, thus impacting the catalytic efficiency of DHP-A. Additionally, Asn37 was observed to undergo fast chemical exchange in DHP-A. This residue is a neighbor of Tyr38, the main tyrosyl radical site in DHP-B as well as in DHP-A at pH 5. We hypothesize that Asn37 interferes with the tyrosyl radical formation at Tyr38 in DHP-A at pH 7, causing the radical to form in Tyr34 instead, thus reducing its catalytic efficiency for peroxidase chemistry. Finally, the distal and proximal histidines are more flexible in DHP-B with 15−18% smaller S^2 values. We have hypothesized that this higher flexibility would facilitate the heterolytic hydrogen peroxide O−O bond cleavage in the formation of compound I in DHP-B as the proximal histidine could move closer to the heme iron in the Fe(IV) state and stabilize it.

https://doi.org/10.1021/acs.jpcb.3c07176
J. Phys. Chem. B 2024, 128, 3383−3397

■ ASSOCIATED CONTENT

Supporting Information

The Supporting Information is available free of charge at https://pubs.acs.org/doi/10.1021/acs.jpcb.3c07176.

Tables showing the comparison of HN, ^{15}N, $^{13}C_{\alpha}$, $^{13}C_{\beta}$, and ^{13}CO chemical shifts and a complete listing of R_1, R_2, and NOEs for DHP-A and DHP-B; figures showing the T_1 and T_2 decays of Phe35 in DHP-A at 19.97 and 16.45 T and MD trajectories of Phe35 (PDF)

■ AUTHOR INFORMATION

Corresponding Author

Stefan Franzen − *Department of Chemistry, North Carolina State University, Raleigh, North Carolina 27695, United States;* orcid.org/0000-0003-2364-2287; Email: franzen@ncsu.edu

Authors

Jessica M. González-Delgado − *Department of Chemistry, North Carolina State University, Raleigh, North Carolina 27695, United States*

Peter M. Thompson − *Department of Molecular and Structural Biochemistry and Molecular Education, Technology and Research Innovation Center (METRIC), North Carolina State University, Raleigh, North Carolina 27695, United States*

Witold Andrałojć − *Institute of Bioorganic Chemistry, Polish Academy of Sciences, 61-704 Poznań, Poland*

Zofia Gdaniec − *Institute of Bioorganic Chemistry, Polish Academy of Sciences, 61-704 Poznań, Poland;* orcid.org/0000-0003-2955-1829

Reza A. Ghiladi − *Department of Chemistry, North Carolina State University, Raleigh, North Carolina 27695, United States*

Complete contact information is available at: https://pubs.acs.org/10.1021/acs.jpcb.3c07176

Notes

The authors declare no competing financial interest.

■ ACKNOWLEDGMENTS

This project was fully supported by the National Science Foundation (CHE-2002954). This work was performed in part by the Molecular Education, Technology and Research Innovation Center (METRIC) at NC State University, which is supported by the State of North Carolina. For the NMR instrumentation, the authors acknowledge Peter M. Thompson and Jennifer Sun from METRIC, Stu Parnham from the Center for Structural Biology at UNC Chapel Hill, and Zofia Gdaniec and Witold Andrałojć from the Polish National Academy of Sciences. Computational resources were provided by the North Carolina State University High Performance Computing Services Core Facility (RRID:SCR_022168). This work was also supported in part by the National Cancer Institute of the National Institutes of Health under award number P30CA016086. J.M.G.D. thanks Dr. Scott Anthony Robson from the Department of Molecular and Cellular Biochemistry at Indiana University for his open-source code libraries and helpful discussions.

■ REFERENCES

(1) Shibayama, N. Allosteric Transitions in Hemoglobin Revisited. *Biochim. Biophys. Acta Gen. Subj.* **2020**, *1864* (2), 129335.

(2) Perutz, M. F.; Wilkinson, A. J.; Paoli, M.; Dodson, G. G. The Stereochemical Mechanism of the Cooperative Effects in Hemoglobin Revisited. *Annu. Rev. Biophys. Biomol. Struct.* **1998**, *27* (1), 1−34.

(3) Zhao, J.; de Serrano, V.; Franzen, S. A Model for the Flexibility of the Distal Histidine in Dehaloperoxidase-Hemoglobin A Based on X-Ray Crystal Structures of the Carbon Monoxide Adduct. *Biochemistry* **2014**, *53* (15), 2474−2482.

(4) Nicoletti, F. P.; Thompson, M. K.; Howes, B. D.; Franzen, S.; Smulevich, G. New Insights into the Role of Distal Histidine Flexibility in Ligand Stabilization of Dehaloperoxidase-Hemoglobin from Amphitrite Ornata. *Biochemistry* **2010**, *49* (9), 1903−1912.

(5) Zhao, J.; de Serrano, V.; Dumarieh, R.; Thompson, M.; Ghiladi, R. A.; Franzen, S. The Role of the Distal Histidine in H2O2 Activation and Heme Protection in Both Peroxidase and Globin Functions. *J. Phys. Chem. B* **2012**, *116* (40), 12065−12077.

(6) Chen, Z.; de Serrano, V.; Betts, L.; Franzen, S. Distal Histidine Conformational Flexibility in Dehaloperoxidase from Amphitrite Ornata. *Acta Crystallogr. D Biol. Crystallogr.* **2009**, *65* (1), 34−40.

(7) Chen, Y. P.; Woodin, S. A.; Lincoln, D. E.; Lovell, C. R. An Unusual Dehalogenating Peroxidase from the Marine Terebellid Polychaete Amphitrite Ornata. *J. Biol. Chem.* **1996**, *271* (9), 4609−4612.

(8) Weber, R. E.; Mangum, C.; Steinman, H.; Bonaventura, C.; Sullivan, B.; Bonaventura, J. Hemoglobins of Two Terebellid Polychaetes: Enoplobranchus Sanguineus and Amphitrite Ornata. *Comp. Biochem. Physiol. A Physiol.* **1977**, *56* (2), 179−187.

(9) Barrios, D. A.; D'Antonio, J.; McCombs, N. L.; Zhao, J.; Franzen, S.; Schmidt, A. C.; Sombers, L. A.; Ghiladi, R. A. Peroxygenase and Oxidase Activities of Dehaloperoxidase-Hemoglobin from Amphitrite Ornata. *J. Am. Chem. Soc.* **2014**, *136* (22), 7914−7925.

(10) Wu, G.; Zhao, J.; Franzen, S.; Tsai, A.-L. Bindings of NO, CO, and O2 to Multifunctional Globin Type Dehaloperoxidase Follow the 'Sliding Scale Rule.'. *Biochem. J.* **2017**, *474* (20), 3485−3498.

(11) Malewschik, T.; de Serrano, V.; McGuire, A. H.; Ghiladi, R. A. The Multifunctional Globin Dehaloperoxidase Strikes Again: Simultaneous Peroxidase and Peroxygenase Mechanisms in the Oxidation of EPA Pollutants. *Arch. Biochem. Biophys.* **2019**, *673*, 108079.

(12) Roach, M. P.; Chen, Y. P.; Woodin, S. A.; Lincoln, D. E.; Lovell, C. R.; Dawson, J. H. Notomastus Lobatus Chloroperoxidase and Amphitrite Ornata Dehaloperoxidase Both Contain Histidine as Their Proximal Heme Iron Ligand. *Biochemistry* **1997**, *36* (8), 2197−2202.

(13) Woodin, S. A.; Walla, M. D.; Lincoln, D. E. Occurrence of Brominated Compounds in Soft-Bottom Benthic Organisms. *J. Exp. Mar. Biol. Ecol.* **1987**, *107* (3), 209−217.

(14) Kringstad, K. P.; Lindstroem, K. Spent Liquors from Pulp Bleaching. *Environ. Sci. Technol.* **1984**, *18* (8), 236A−248A.

(15) Han, K.; Woodin, S. A.; Lincoln, D. E.; Fielman, K. T.; Ely, B. Amphitrite Ornata, a Marine Worm, Contains Two Dehaloperoxidase Genes. *Mar. Biotechnol.* **2001**, *3* (3), 287−292.

(16) D'Antonio, J.; D'Antonio, E. L.; Thompson, M. K.; Bowden, E. F.; Franzen, S.; Smirnova, T.; Ghiladi, R. A. Spectroscopic and Mechanistic Investigations of Dehaloperoxidase B from Amphitrite Ornata. *Biochemistry* **2010**, *49* (31), 6600−6616.

(17) Le, P.; Zhao, J.; Franzen, S. Correlation of Heme Binding Affinity and Enzyme Kinetics of Dehaloperoxidase. *Biochemistry* **2014**, *53* (44), 6863−6877.

(18) Aktar, M. S.; de Serrano, V.; Ghiladi, R.; Franzen, S. Comparative Study of the Binding and Activation of 2,4-Dichlorophenol by Dehaloperoxidase A and B. *J. Inorg. Biochem.* **2023**, *247*, 112332.

(19) Franzen, S.; Ghiladi, R. A.; Lebioda, L.; Dawson, J. Multi-Functional Hemoglobin Dehaloperoxidases. In *Heme Peroxidases*; The Royal Society of Chemistry, 2016; Vol. *2016*, pp 218−244.

(20) Smirnova, T. I.; Weber, R. T.; Davis, M. F.; Franzen, S. Substrate Binding Triggers a Switch in the Iron Coordination in Dehaloperoxidase from Amphitrite Ornata: HYSCORE Experiments. *J. Am. Chem. Soc.* **2008**, *130* (7), 2128−2129.
(21) Thompson, M. K.; Davis, M. F.; de Serrano, V.; Nicoletti, F. P.; Howes, B. D.; Smulevich, G.; Franzen, S. Internal Binding of Halogenated Phenols in Dehaloperoxidase-Hemoglobin Inhibits Peroxidase Function. *Biophys. J.* **2010**, *99* (5), 1586−1595.
(22) Davis, M. F.; Gracz, H.; Vendeix, F. A. P.; de Serrano, V.; Somasundaram, A.; Decatur, S. M.; Franzen, S. Different Modes of Binding of Mono-, Di-, and Trihalogenated Phenols to the Hemoglobin Dehaloperoxidase from Amphitrite Ornata. *Biochemistry* **2009**, *48* (10), 2164−2172.
(23) Nienhaus, K.; Nickel, E.; Davis, M. F.; Franzen, S.; Nienhaus, G. U. Determinants of Substrate Internalization in the Distal Pocket of Dehaloperoxidase Hemoglobin of Amphitrite Ornata. *Biochemistry* **2008**, *47* (49), 12985−12994.
(24) de Serrano, V.; Chen, Z.; Davis, M. F.; Franzen, S. X-Ray Crystal Structural Analysis of the Binding Site in the Ferric and Oxyferrous Forms of the Recombinant Heme Dehaloperoxidase Cloned from Amphitrite Ornata. *Acta Crystallogr. D Biol. Crystallogr.* **2007**, *63* (10), 1094−1101.
(25) McCombs, N. L.; D'Antonio, J.; Barrios, D. A.; Carey, L. M.; Ghiladi, R. A. Nonmicrobial Nitrophenol Degradation via Peroxygenase Activity of Dehaloperoxidase-Hemoglobin from Amphitrite Ornata. *Biochemistry* **2016**, *55* (17), 2465−2478.
(26) McCombs, N. L.; Moreno-Chicano, T.; Carey, L. M.; Franzen, S.; Hough, M. A.; Ghiladi, R. A. Interaction of Azole-Based Environmental Pollutants with the Coelomic Hemoglobin from Amphitrite Ornata: A Molecular Basis for Toxicity. *Biochemistry* **2017**, *56* (17), 2294−2303.
(27) Schkolnik, G.; Utesch, T.; Zhao, J.; Jiang, S.; Thompson, M. K.; Mroginski, M.-A.; Hildebrandt, P.; Franzen, S. Catalytic Efficiency of Dehaloperoxidase A Is Controlled by Electrostatics - Application of the Vibrational Stark Effect to Understand Enzyme Kinetics. *Biochem. Biophys. Res. Commun.* **2013**, *430* (3), 1011−1015.
(28) Franzen, S.; Belyea, J.; Gilvey, L. B.; Davis, M. F.; Chaudhary, C. E.; Sit, T. L.; Lommel, S. A. Proximal Cavity, Distal Histidine, and Substrate Hydrogen-Bonding Mutations Modulate the Activity of Amphitrite Ornata Dehaloperoxidase. *Biochemistry* **2006**, *45* (30), 9085−9094.
(29) D'Antonio, E. L.; D'Antonio, J.; de Serrano, V.; Gracz, H.; Thompson, M. K.; Ghiladi, R. A.; Bowden, E. F.; Franzen, S. Functional Consequences of the Creation of an Asp-His-Fe Triad in a 3/3 Globin. *Biochemistry* **2011**, *50* (44), 9664−9680.
(30) Jiang, S.; Wright, I.; Swartz, P.; Franzen, S. The Role of T56 in Controlling the Flexibility of the Distal Histidine in Dehaloperoxidase-Hemoglobin from Amphitrite Ornata. *Biochim. Biophys. Acta BBA - Proteins Proteomics* **2013**, *1834* (10), 2020−2029.
(31) Carey, L. M.; Gavenko, R.; Svistunenko, D. A.; Ghiladi, R. A. How Nature Tunes Isoenzyme Activity in the Multifunctional Catalytic Globin Dehaloperoxidase from Amphitrite Ornata. *Biochim. Biophys. Acta BBA - Proteins Proteomics* **2018**, *1866* (2), 230−241.
(32) Dumarieh, R.; D'Antonio, J.; Deliz-Liang, A.; Smirnova, T.; Svistunenko, D. A.; Ghiladi, R. A. Tyrosyl Radicals in Dehaloperoxidase. *J. Biol. Chem.* **2013**, *288* (46), 33470−33482.
(33) Davydov, R.; Osborne, R. L.; Shanmugam, M.; Du, J.; Dawson, J. H.; Hoffman, B. M. Probing the Oxyferrous and Catalytically Active Ferryl States of Amphitrite Ornata Dehaloperoxidase by Cryoreduction and EPR/ENDOR Spectroscopy. Detection of Compound I. *J. Am. Chem. Soc.* **2010**, *132* (42), 14995−15004.
(34) Thompson, M. K.; Franzen, S.; Ghiladi, R. A.; Reeder, B. J.; Svistunenko, D. A. Compound ES of Dehaloperoxidase Decays via Two Alternative Pathways Depending on the Conformation of the Distal Histidine. *J. Am. Chem. Soc.* **2010**, *132* (49), 17501−17510.
(35) Kleckner, I. R.; Foster, M. P. An Introduction to NMR-Based Approaches for Measuring Protein Dynamics. *Biochim. Biophys. Acta* **2011**, *1814* (8), 942−968.
(36) d'Auvergne, E. J.; Gooley, P. R. Set Theory Formulation of the Model-Free Problem and the Diffusion Seeded Model-Free Paradigm. *Mol. Biosyst.* **2007**, *3* (7), 483−494.
(37) Palmer, A. G. Enzyme Dynamics from NMR Spectroscopy. *Acc. Chem. Res.* **2015**, *48* (2), 457−465.
(38) Kay, L. E. Protein Dynamics from NMR. *Nat. Struct. Biol.* **1998**, *5* (7), 513−517.
(39) Palmer, A. G.; Williams, J.; McDermott, A. Nuclear Magnetic Resonance Studies of Biopolymer Dynamics. *J. Phys. Chem.* **1996**, *100* (31), 13293−13310.
(40) Tozawa, K.; Ferguson, S. J.; Redfield, C.; Smith, L. J. Comparison of the Backbone Dynamics of Wild-Type Hydrogenobacter Thermophilus Cytochrome C552 and Its b-Type Variant. *J. Biomol. NMR* **2015**, *62* (2), 221−231.
(41) Karsisiotis, A. I.; Deacon, O. M.; Wilson, M. T.; Macdonald, C.; Blumenschein, T. M. A.; Moore, G. R.; Worrall, J. A. R. Increased Dynamics in the 40−57 Ω-Loop of the G41S Variant of Human Cytochrome c Promote Its pro-Apoptotic Conformation. *Sci. Rep.* **2016**, *6* (1), 30447.
(42) Harada, E.; Sugishima, M.; Harada, J.; Fukuyama, K.; Sugase, K. Distal Regulation of Heme Binding of Heme Oxygenase-1 Mediated by Conformational Fluctuations. *Biochemistry* **2015**, *54* (2), 340−348.
(43) Muthu, D.; Berry, R. E.; Zhang, H.; Walker, F. A. NMR Studies of the Dynamics of Nitrophorin 2 Bound to Nitric Oxide. *Biochemistry* **2013**, *52* (45), 7910−7925.
(44) Stetz, M. A.; Caro, J. A.; Kotaru, S.; Yao, X.; Marques, B. S.; Valentine, K. G.; Wand, A. J. Characterization of Internal Protein Dynamics and Conformational Entropy by NMR Relaxation. In *Methods in Enzymology*; Academic Press, 2019; Vol. *615*, pp 237−284.
(45) Kocman, V.; Di Mauro, G. M.; Veglia, G.; Ramamoorthy, A. Use of Paramagnetic Systems to Speed-up NMR Data Acquisition and for Structural and Dynamic Studies. *Solid State Nucl. Magn. Reson.* **2019**, *102*, 36−46.
(46) Song, X.; Yuan, Y.; Simplaceanu, V.; Sahu, S. C.; Ho, N. T.; Ho, C. A Comparative NMR Study of the Polypeptide Backbone Dynamics of Hemoglobin in the Deoxy and Carbonmonoxy Forms. *Biochemistry* **2007**, *46* (23), 6795−6803.
(47) Laine, J. M.; Amat, M.; Morgan, B. R.; Royer, W. E.; Massi, F. Insight into the Allosteric Mechanism of Scapharca Dimeric Hemoglobin. *Biochemistry* **2014**, *53* (46), 7199−7210.
(48) Preimesberger, M. R.; Majumdar, A.; Lecomte, J. T. J. Dynamics of Lysine as a Heme Axial Ligand: NMR Analysis of the Chlamydomonas Reinhardtii Hemoglobin THB1. *Biochemistry* **2017**, *56* (4), 551−569.
(49) Longeville, S.; Stingaciu, L.-R. Hemoglobin Diffusion and the Dynamics of Oxygen Capture by Red Blood Cells. *Sci. Rep.* **2017**, *7* (1), 10448.
(50) Davis, M. F.; Bobay, B. G.; Franzen, S. Determination of Separate Inhibitor and Substrate Binding Sites in the Dehaloperoxidase-Hemoglobin from Amphitrite Ornata. *Biochemistry* **2010**, *49* (6), 1199−1206.
(51) Zhao, J.; Xue, M.; Gudanis, D.; Gracz, H.; Findenegg, G. H.; Gdaniec, Z.; Franzen, S. Dynamics of Dehaloperoxidase-Hemoglobin A Derived from NMR Relaxation Spectroscopy and Molecular Dynamics Simulation. *J. Inorg. Biochem.* **2018**, *181*, 65−73.
(52) Cai, M.; Huang, Y.; Sakaguchi, K.; Clore, G. M.; Gronenborn, A. M.; Craigie, R. An Efficient and Cost-Effective Isotope Labeling Protocol for Proteins Expressed in Escherichia Coli. *J. Biomol. NMR* **1998**, *11* (1), 97−102.
(53) Belyea, J.; Gilvey, L. B.; Davis, M. F.; Godek, M.; Sit, T. L.; Lommel, S. A.; Franzen, S. Enzyme Function of the Globin Dehaloperoxidase from Amphitrite Ornata Is Activated by Substrate Binding. *Biochemistry* **2005**, *44* (48), 15637−15644.
(54) Osborne, R. L.; Sumithran, S.; Coggins, M. K.; Chen, Y.-P.; Lincoln, D. E.; Dawson, J. H. Spectroscopic Characterization of the Ferric States of Amphitrite Ornata Dehaloperoxidase and Notomastus Lobatus Chloroperoxidase: His-Ligated Peroxidases with Globin-like Proximal and Distal Properties. *J. Inorg. Biochem.* **2006**, *100* (5−6), 1100−1108.

https://doi.org/10.1021/acs.jpcb.3c07176
J. Phys. Chem. B 2024, 128, 3383−3397

(55) Hwang, T.-L.; Shaka, A. J. Water Suppression That Works. Excitation Sculpting Using Arbitrary Wave-Forms and Pulsed-Field Gradients. *J. Magn. Reson. A* **1995**, *112*, 275−279.
(56) Schleucher, J.; Sattler, M.; Griesinger, C. Coherence Selection by Gradients without Signal Attenuation: Application to the Three Dimensional HNCO Experiment. *Angew. Chem., Int. Ed. Engl.* **1993**, *32* (10), 1489−1491.
(57) Kay, L. E.; Xu, G. Y.; Yamazaki, T. Enhanced-Sensitivity Triple-Resonance Spectroscopy with Minimal H2O Saturation. *J. Magn. Reson. A* **1994**, *109*, 129−133.
(58) Grzesiek, S.; Bax, A. Improved 3D Triple-Resonance NMR Techniques Applied to a 31 kDa Protein. *J. Magn. Reson. 1969* **1992**, *96*, 432−440.
(59) Muhandiram, D. R.; Kay, L. E. Gradient-Enhanced Triple-Resonance Three-Dimensional NMR Experiments with Improved Sensitivity. *J. Magn. Reson. B* **1994**, *103*, 203−216.
(60) Wittekind, M.; Mueller, L. HNCACB, a High-Sensitivity 3D NMR Experiment to Correlate Amide-Proton and Nitrogen Resonances with the Alpha- and Beta-Carbon Resonances in Proteins. *J. Magn. Reson. B* **1993**, *101*, 201−205.
(61) Grzesiek, S.; Bax, A. Amino Acid Type Determination in the Sequential Assignment Procedure of Uniformly 13C/15N-Enriched Proteins. *J. Biomol. NMR* **1993**, *3*, 185−204.
(62) Schleucher, J.; Schwendinger, M.; Sattler, M.; Schmidt, P.; Schedletzky, O.; Glaser, S. J.; Sorensen, O. W.; Griesinger, C. A General Enhancement Scheme in Heteronuclear Multidimensional NMR Employing Pulsed Field Gradients. *J. Biomol. NMR* **1994**, *4*, 301−306.
(63) Kay, L.; Keifer, P.; Saarinen, T. Pure Absorption Gradient Enhanced Heteronuclear Single Quantum Correlation Spectroscopy with Improved Sensitivity. *J. Am. Chem. Soc.* **1992**, *114*, 10663−10665.
(64) Palmer, A. G.; Cavanagh, J.; Wright, P. E.; Rance, M. Sensitivity Improvement in Proton-Detected Two-Dimensional Heteronuclear Correlation NMR Spectroscopy. *J. Magn. Reson.* **1991**, *93*, 151−170.
(65) Delaglio, F.; Grzesiek, S.; Vuister, G..; Zhu, G.; Pfeifer, J.; Bax, A. NMRPipe: A Multidimensional Spectral Processing System Based on UNIX Pipes. *J. Biomol. NMR* **1995**, *6* (3), 293.
(66) Lee, W.; Tonelli, M.; Markley, J. L. NMRFAM-SPARKY: Enhanced Software for Biomolecular NMR Spectroscopy. *Bioinformatics* **2015**, *31* (8), 1325−1327.
(67) Lee, W.; Rahimi, M.; Lee, Y.; Chiu, A. POKY: A Software Suite for Multidimensional NMR and 3D Structure Calculation of Biomolecules. *Bioinformatics* **2021**, *37* (18), 3041−3042.
(68) Lipari, G.; Szabo, A. Model-Free Approach to the Interpretation of Nuclear Magnetic Resonance Relaxation in Macromolecules. 1. Theory and Range of Validity. *J. Am. Chem. Soc.* **1982**, *104* (17), 4546−4559.
(69) Lipari, G.; Szabo, A. Model-Free Approach to the Interpretation of Nuclear Magnetic Resonance Relaxation in Macromolecules. 2. Analysis of Experimental Results. *J. Am. Chem. Soc.* **1982**, *104* (17), 4559−4570.
(70) Clore, G. M.; Szabo, A.; Bax, A.; Kay, L. E.; Driscoll, P. C.; Gronenborn, A. M. Deviations from the Simple Two-Parameter Model-Free Approach to the Interpretation of Nitrogen-15 Nuclear Magnetic Relaxation of Proteins. *J. Am. Chem. Soc.* **1990**, *112* (12), 4989−4991.
(71) Cole, R.; Loria, J. P. FAST-Modelfree: A Program for Rapid Automated Analysis of Solution NMR Spin-Relaxation Data. *J. Biomol. NMR* **2003**, *26*, 203−213.
(72) Peng, J. W.; Wagner, G. Mapping of Spectral Density Functions Using Heteronuclear NMR Relaxation Measurements. *J. Magn. Reson.* **1992**, *98* (2), 308−332.
(73) Palmer III, A. G. NMR Probes of Molecular Dynamics: Overview and Comparison with Other Techniques. *Annu. Rev. Biophys. Biomol. Struct.* **2001**, *30* (1), 129−155.
(74) d'Auvergne, E. J.; Gooley, P. R. Optimisation of NMR Dynamic Models I. Minimisation Algorithms and Their Performance within the Model-Free and Brownian Rotational Diffusion Spaces. *J. Biomol. NMR* **2008**, *40* (2), 107.
(75) d'Auvergne, E. J.; Gooley, P. R. Optimisation of NMR Dynamic Models II. A New Methodology for the Dual Optimisation of the Model-Free Parameters and the Brownian Rotational Diffusion Tensor. *J. Biomol. NMR* **2008**, *40* (2), 121−133.
(76) Bae, S.-H.; Legname, G.; Serban, A.; Prusiner, S. B.; Wright, P. E.; Dyson, H. J. Prion Proteins with Pathogenic and Protective Mutations Show Similar Structure and Dynamics. *Biochemistry* **2009**, *48* (34), 8120−8128.
(77) Phillips, J. C.; Braun, R.; Wang, W.; Gumbart, J.; Tajkhorshid, E.; Villa, E.; Chipot, C.; Skeel, R. D.; Kalé, L.; Schulten, K. Scalable Molecular Dynamics with NAMD. *J. Comput. Chem.* **2005**, *26* (16), 1781−1802.
(78) Hatcher, E. R.; Guvench, O.; MacKerell, A. D. CHARMM Additive All-Atom Force Field for Acyclic Polyalcohols, Acyclic Carbohydrates, and Inositol. *J. Chem. Theory Comput.* **2009**, *5* (5), 1315−1327.
(79) Klauda, J. B.; Monje, V.; Kim, T.; Im, W. Improving the CHARMM Force Field for Polyunsaturated Fatty Acid Chains. *J. Phys. Chem. B* **2012**, *116* (31), 9424−9431.
(80) Best, R. B.; Zhu, X.; Shim, J.; Lopes, P. E. M.; Mittal, J.; Feig, M.; Mackerell, A. D. Optimization of the Additive CHARMM All-Atom Protein Force Field Targeting Improved Sampling of the Backbone φ, ψ and Side-Chain X1 and X2 Dihedral Angle. *J. Chem. Theory Comput.* **2012**, *8* (9), 3257−3273.
(81) Yu, W.; He, X.; Vanommeslaeghe, K.; MacKerell, A. D. Extension of the CHARMM General Force Field to Sulfonyl-Containing Compounds and Its Utility in Biomolecular Simulations. *J. Comput. Chem.* **2012**, *33* (31), 2451−2468.
(82) Klauda, J. B.; Venable, R. M.; Freites, J. A.; O'Connor, J. W.; Tobias, D. J.; Mondragon-Ramirez, C.; Vorobyov, I.; MacKerell, A. D.; Pastor, R. W. Update of the CHARMM All-Atom Additive Force Field for Lipids: Validation on Six Lipid Types. *J. Phys. Chem. B* **2010**, *114* (23), 7830−7843.
(83) Guvench, O.; Hatcher, E.; Venable, R. M.; Pastor, R. W.; MacKerell, A. D. CHARMM Additive All-Atom Force Field for Glycosidic Linkages between Hexopyranoses. *J. Chem. Theory Comput.* **2009**, *5* (9), 2353−2370.
(84) Guvench, O.; Mallajosyula, S. S.; Raman, E. P.; Hatcher, E.; Vanommeslaeghe, K.; Foster, T. J.; Jamison, F. W.; MacKerell, A. D. CHARMM Additive All-Atom Force Field for Carbohydrate Derivatives and Its Utility in Polysaccharide and Carbohydrate-Protein Modeling. *J. Chem. Theory Comput.* **2011**, *7* (10), 3162−3180.
(85) Hatcher, E.; Guvench, O.; MacKerell, A. D. CHARMM Additive All-Atom Force Field for Aldopentofuranoses, Methyl-Aldopentofuranosides, and Fructofuranose. *J. Phys. Chem. B* **2009**, *113* (37), 12466−12476.
(86) Stote, R. H.; Karplus, M. Zinc Binding in Proteins and Solution: A Simple but Accurate Nonbonded Representation. *Proteins Struct. Funct. Genet.* **1995**, *23* (1), 12−31.
(87) Li, Z.-W.; Sun, Z.-Y.; Lu, Z.-Y. Simulation Model for Hierarchical Self-Assembly of Soft Disklike Particles. *J. Phys. Chem. B* **2010**, *114* (7), 2353−2358.
(88) MacKerell, A. D.; Bashford, D.; Bellott, M.; Dunbrack, R. L.; Evanseck, J. D.; Field, M. J.; Fischer, S.; Gao, J.; Guo, H.; Ha, S.; et al. All-Atom Empirical Potential for Molecular Modeling and Dynamics Studies of Proteins. *J. Phys. Chem. B* **1998**, *102* (18), 3586−3616.
(89) Mallajosyula, S. S.; Guvench, O.; Hatcher, E.; MacKerell, A. D. CHARMM Additive All-Atom Force Field for Phosphate and Sulfate Linked to Carbohydrates. *J. Chem. Theory Comput.* **2012**, *8* (2), 759−776.
(90) Beglov, D.; Roux, B. Finite Representation of an Infinite Bulk System: Solvent Boundary Potential for Computer Simulations. *J. Chem. Phys.* **1994**, *100* (12), 9050−9063.
(91) Mallajosyula, S. S.; MacKerell, A. D. Influence of Solvent and Intramolecular Hydrogen Bonding on the Conformational Properties of O-Linked Glycopeptides. *J. Phys. Chem. B* **2011**, *115* (38), 11215−11229.

https://doi.org/10.1021/acs.jpcb.3c07176
J. Phys. Chem. B 2024, 128, 3383−3397

(92) MacKerell, A. D.; Feig, M.; Brooks, C. L. Improved Treatment of the Protein Backbone in Empirical Force Fields. *J. Am. Chem. Soc.* **2004**, *126* (3), 698−699.
(93) Jorgensen, W. L.; Chandrasekhar, J.; Madura, J. D.; Impey, R. W.; Klein, M. L. Comparison of Simple Potential Functions for Simulating Liquid Water. *J. Chem. Phys.* **1983**, *79* (2), 926−935.
(94) Farrow, N. A.; Muhandiram, R.; Singer, A. U.; Pascal, S. M.; Kay, C. M.; Gish, G.; Shoelson, S. E.; Pawson, T.; Forman-Kay, J. D.; Kay, L. E. Backbone Dynamics of a Free and a Phosphopeptide-Complexed Src Homology 2 Domain Studied by 15N NMR Relaxation. *Biochemistry* **1994**, *33* (19), 5984−6003.
(95) Guvench, O.; Greene, S. N.; Kamath, G.; Brady, J. W.; Venable, R. M.; Pastor, R. W.; Mackerell, A. D. Additive Empirical Force Field for Hexopyranose Monosaccharides. *J. Comput. Chem.* **2008**, *29* (15), 2543−2564.
(96) Vanommeslaeghe, K.; Hatcher, E.; Acharya, C.; Kundu, S.; Zhong, S.; Shim, J.; Darian, E.; Guvench, O.; Lopes, P.; Vorobyov, I.; Mackerell, A. D. CHARMM General Force Field: A Force Field for Drug-like Molecules Compatible with the CHARMM All-Atom Additive Biological Force Fields. *J. Comput. Chem.* **2010**, *31* (4), 671.
(97) Darden, T.; York, D.; Pedersen, L. Particle Mesh Ewald: An N·log(N) Method for Ewald Sums in Large Systems. *J. Chem. Phys.* **1993**, *98* (12), 10089−10092.
(98) Glykos, N. M. Software News and Updates Carma: A Molecular Dynamics Analysis Program. *J. Comput. Chem.* **2006**, *27* (14), 1765−1768.
(99) Brooks, B. R.; Bruccoleri, R. E.; Olafson, B. D.; States, D. J.; Swaminathan, S.; Karplus, M. CHARMM: A Program for Macromolecular Energy, Minimization, and Dynamics Calculations. *J. Comput. Chem.* **1983**, *4* (2), 187−217.
(100) MacKerell, A. D.; Brooks, B.; Brooks, C. L.; Nilsson, L.; Roux, B.; Won, Y.; Karplus, M. CHARMM: The Energy Function and Its Parameterization. In *Encyclopedia of Computational Chemistry*; John Wiley & Sons: Chichester, U.K., 2002 DOI: 10.1002/0470845015.cfa007.
(101) Brooks, B. R.; Brooks, C. L.; Mackerell, A. D.; Nilsson, L.; Petrella, R. J.; Roux, B.; Won, Y.; Archontis, G.; Bartels, C.; Boresch, S.; et al. CHARMM: The Biomolecular Simulation Program. *J. Comput. Chem.* **2009**, *30* (10), 1545−1614.
(102) Anthis, N. J.; Clore, G. M. Visualizing Transient Dark States by NMR Spectroscopy. *Q. Rev. Biophys.* **2015**, *48* (1), 35−116.
(103) Woessner, D. E. Brownian Motion and Its Effects in NMR Chemical Exchange and Relaxation in Liquids. *Concepts Magn. Reson.* **1996**, *8* (6), 397−421.
(104) Levy, R. M.; Karplus, M.; Wolynes, P. G. NMR Relaxation Parameters in Molecules with Internal Motion: Exact Langevin Trajectory Results Compared with Simplified Relaxation Models. *J. Am. Chem. Soc.* **1981**, *103* (20), 5998−6011.
(105) Farrow, N. A.; Zhang, O.; Szabo, A.; Torchia, D. A.; Kay, L. E. Spectral Density Function Mapping Using 15N Relaxation Data Exclusively. *J. Biomol. NMR* **1995**, *6* (2), 153−162.
(106) Morin, S.; Gagné, S. M. Simple Tests for the Validation of Multiple Field Spin Relaxation Data. *J. Biomol. NMR* **2009**, *45* (4), 361−372.
(107) Palmer, A. G.; Koss, H. Chemical Exchange. In *Methods in Enzymology*; Academic Press, 2019; Vol. *615*, pp 177−236 DOI: 10.1016/bs.mie.2018.09.028.
(108) Jen, J. Chemical Exchange and NMR-T2 Relaxation. *Adv. Mol. Relax. Process.* **1974**, *6* (2), 171−183.
(109) Kroenke, C. D.; Loria, J. P.; Lee, L. K.; Rance, M.; Palmer, A. G. Longitudinal and Transverse 1H-15N Dipolar/15N Chemical Shift Anisotropy Relaxation Interference: Unambiguous Determination of Rotational Diffusion Tensors and Chemical Exchange Effects in Biological Macromolecules. *J. Am. Chem. Soc.* **1998**, *120* (31), 7905−7915.
(110) Robson, S. A.; Dag, Ç.; Wu, H.; Ziarek, J. J. TRACT Revisited: An Algebraic Solution for Determining Overall Rotational Correlation Times from Cross-Correlated Relaxation Rates. *J. Biomol. NMR* **2021**, *75* (8−9), 293−302.
(111) Wommack, A. J.; Robson, S. A.; Wanniarachchi, Y. A.; Wan, A.; Turner, C. J.; Wagner, G.; Nolan, E. M. NMR Solution Structure and Condition-Dependent Oligomerization of the Antimicrobial Peptide Human Defensin 5. *Biochemistry* **2012**, *51* (48), 9624−9637.
(112) Robson, S. A.; Jacobitz, A. W.; Phillips, M. L.; Clubb, R. T. Solution Structure of the Sortase Required for Efficient Production of Infectious Bacillus Anthracis Spores. *Biochemistry* **2012**, *51* (40), 7953−7963.
(113) Olejniczak, E. T.; Dobson, C. M.; Karplus, M.; Levy, R. M. Motional Averaging of Proton Nuclear Overhauser Effects in Proteins. Predictions from a Molecular Dynamics Simulation of Lysozyme. *J. Am. Chem. Soc.* **1984**, *106* (7), 1923−1930.
(114) Morin, S. A Practical Guide to Protein Dynamics from 15N Spin Relaxation in Solution. *Prog. Nucl. Magn. Reson. Spectrosc.* **2011**, *59* (3), 245−262.
(115) Zhang, L.; Bouguet-Bonnet, S.; Buck, M. Combining NMR and Molecular Dynamics Studies for Insights into the Allostery of Small GTPase-Protein Interactions. In *Methods in Molecular Biology*; Springer, 2012; Vol. *796*, pp 235−259.
(116) de Serrano, V. S.; Davis, M. F.; Gaff, J. F.; Zhang, Q.; Chen, Z.; D'Antonio, E. L.; Bowden, E. F.; Rose, R.; Franzen, S. X-Ray Structure of the Metcyano Form of Dehaloperoxidase from Amphitriteornata: Evidence for Photoreductive Dissociation of the Iron-Cyanide Bond. *Acta Crystallogr. D Biol. Crystallogr.* **2010**, *66* (7), 770−782.
(117) Zhao, J.; Moretto, J.; Le, P.; Franzen, S. Measurement of Internal Substrate Binding in Dehaloperoxidase-Hemoglobin by Competition with the Heme-Fluoride Binding Equilibrium. *J. Phys. Chem. B* **2015**, *119* (7), 2827−2838.
(118) Saitô, H. Dynamic Pictures of Proteins by NMSR. *Annual Reports on NMR Spectroscopy*; Academic Press, 2014; Vol. *83*, pp 1−66.
(119) Thompson, M. K.; Franzen, S.; Davis, M. F.; Oliver, R. C.; Krueger, J. K. Dehaloperoxidase-Hemoglobin from Amphitrite Ornata Is Primarily a Monomer in Solution. *J. Phys. Chem. B* **2011**, *115* (14), 4266−4272.
(120) de Serrano, V.; D'Antonio, J.; Franzen, S.; Ghiladi, R. A. Structure of Dehaloperoxidase B at 1.58 Å Resolution and Structural Characterization of the AB Dimer from Amphitrite Ornata. *Acta Crystallogr. D Biol. Crystallogr.* **2010**, *66* (5), 529−538.
(121) Cai, Y.; Kurt Yilmaz, N.; Myint, W.; Ishima, R.; Schiffer, C. A. Differential Flap Dynamics in Wild-Type and a Drug Resistant Variant of HIV-1 Protease Revealed by Molecular Dynamics and NMR Relaxation. *J. Chem. Theory Comput.* **2012**, *8* (10), 3452−3462.
(122) Ishima, R.; Louis, J. M. A Diverse View of Protein Dynamics from NMR Studies of HIV-1 Protease Flaps. *Proteins Struct. Funct. Bioinforma.* **2008**, *70* (4), 1408−1415.
(123) Olivieri, C.; Walker, C.; Veliparambil Subrahmanian, M.; Porcelli, F.; Taylor, S. S.; Bernlohr, D. A.; Veglia, G. An NMR Portrait of Functional and Dysfunctional Allosteric Cooperativity in cAMP-Dependent Protein Kinase A. *FEBS Lett.* **2023**, *597* (8), 1055−1072.
(124) Feducia, J.; Dumarieh, R.; Gilvey, L. B. G.; Smirnova, T.; Franzen, S.; Ghiladi, R. A. Characterization of Dehaloperoxidase Compound ES and Its Reactivity with Trihalophenols. *Biochemistry* **2009**, *48* (5), 995−1005.
(125) Tsaprailis, G.; English, A. M. Different Pathways of Radical Translocation in Yeast Cytochrome c Peroxidase and Its W191F Mutant on Reaction with H2O2 Suggest an Antioxidant Role. *JBIC J. Biol. Inorg. Chem.* **2003**, *8* (3), 248−255.
(126) Poulos, T. L.; Kraut, J. The Stereochemistry of Peroxidase Catalysis. *J. Biol. Chem.* **1980**, *255* (17), 8199−8205.

https://doi.org/10.1021/acs.jpcb.3c07176
J. Phys. Chem. B 2024, 128, 3383−3397